Analytical Biochemistry 529 (2017) 245–269

Contents lists available at ScienceDirect

Analytical Biochemistry

journal homepage: www.elsevier.com/locate/yabio

MRS studies of neuroenergetics and glutamate/glutamine exchange in rats: Extensions to hyperammonemic models

Bernard Lanz [a, b, *], Veronika Rackayova [a], Olivier Braissant [c], Cristina Cudalbu [d]

[a] Laboratory for Functional and Metabolic Imaging (LIFMET), Ecole Polytechnique Fédérale de Lausanne (EPFL), Lausanne, Switzerland
[b] Sir Peter Mansfield Imaging Centre, School of Physics and Astronomy, University of Nottingham, Nottingham, United Kingdom
[c] Service of Biomedicine, Neurometabolic Unit, Lausanne University Hospital, Lausanne, Switzerland
[d] Centre d'Imagerie Biomédicale (CIBM), Ecole Polytechnique Fédérale de Lausanne (EPFL), Lausanne, Switzerland

ARTICLE INFO

Article history:
Received 13 August 2016
Received in revised form
16 November 2016
Accepted 30 November 2016
Available online 23 December 2016

Keywords:
In vivo magnetic resonance spectroscopy
Brain metabolism
Neuroenergetics
Glutamate/glutamine cycle
Hyperammonemia

ABSTRACT

In vivo Magnetic Resonance Spectroscopy is a useful tool to characterize brain biochemistry as well as its alteration in a large number of major central nervous system diseases. The present review will focus on the study of the glutamate-glutamine cycle, an important biochemical pathway in excitatory neurotransmission, analyzed using *in vivo* MRS of different accessible nuclei: ^{1}H, ^{13}C, ^{15}N and ^{31}P. The different methodological aspects of data acquisition, processing and absolute quantification of the MRS data for each nucleus will be presented, as well as the description of the mathematical modeling approach to interpret the MRS measurements in terms of biochemical kinetics. The unique advantages of MRS, especially its non-invasive nature enabling longitudinal monitoring of brain disease progression and/or effect of treatment is illustrated in the particular context of hyperammonemic disorders with a specific focus on animal models. We review the current possibilities given by *in vivo* MRS to investigate some of the molecular mechanisms involved in hyperammonemic disorders and to give a better understanding of the process of development of hepatic encephalopathy, a severe neuropsychiatric disorder that frequently accompanies liver disease.

1. Introduction

Compared to magnetic resonance imaging (MRI), where the output consists of an image in a grey scale, MR spectroscopy (MRS) provides a spectrum as readout. This spectrum consists of peaks at different resonant frequencies (or resonances) representing signal intensities. Resonant frequency is often expressed in parts per million (ppm), which is the magnetic field independent frequency scale. When performing single voxel MRS, spectra are acquired from a well-defined single volume, usually positioned in a specific brain region. In spectroscopic imaging (MRSI), also called chemical shift imaging (CSI), spectra are simultaneously acquired from different brain regions and thus the spatial distribution of metabolites in various regions of the brain can be efficiently studied. After quantification of the entire set of acquired spectra, each acquired from different spatial positions (volumes), the result is usually displayed as a metabolic map (images of individual metabolite concentrations using a grey or colored scale from the lowest to the highest concentration). Spectroscopic imaging can be performed in rodents with μL spatial resolution, which is comparable in resolution to animal positron emission tomography (PET) [1], or even better.

In vivo MRS is a powerful and reliable diagnostic tool with unique advantages due to its non-invasiveness and consequently its possibility to be used in a longitudinal manner. It thus enables the monitoring of disease progression and/or effect of treatment, and makes a bridge between the clinical diagnostics and basic research. *In vivo* studies of energy metabolism and/or glutamate-glutamine cycle can be performed using different nuclei (^{1}H, ^{31}P, ^{13}C, ^{15}N, ^{17}O). These studies can be more or less complex depending on the nuclei under investigation. Fig. 1 shows an example of representative ^{1}H, ^{31}P, ^{13}C and ^{15}N spectra acquired *in vivo* in the rat brain. As can be seen, all these spectra look quite different. However, since the majority of organic compounds contain hydrogen, carbon and also nitrogen or phosphorus, these spectra often offer complementary information on the same metabolites by detecting different atoms in the molecule (e.g. phosphocreatine in ^{1}H and ^{31}P

* Corresponding author. Sir Peter Mansfield Imaging Centre, School of Physics and Astronomy, University of Nottingham, Nottingham, United Kingdom.
E-mail address: bernard.lanz@nottingham.ac.uk (B. Lanz).

http://dx.doi.org/10.1016/j.ab.2016.11.021
0003-2697/

Abbreviations

ADP	adenosine diphosphate
AHP	adiabatic half passage
Ala	alanine
ALF	acute liver failure
AMARES	Advanced Method for Accurate, Robust, and Efficient Spectral fitting
Asc	ascorbate
Asp	aspartate
ATP	adenosine triphosphate
BBB	blood-brain-barrier
BDL	bile duct ligation
CK	creatine kinase
CLD	chronic liver disease
Cr	creatine
CRLB	Cramér-Rao lower bounds
CSI	chemical shift imaging
GABA	γ-aminobutyrate
Glc	glucose
Gln	glutamine
Glu	glutamate
GLUTs	glucose transporters
Gly	glycine
GPC	glycerophosphocholine
GS	glutamine synthetase
GSH	glutathione
HA	hyperammonemia
HE	hepatic encephalopathy
Ins	myo-inositol
Lac	lactate
MCTs	monocarboxylate transporters
MRI	magnetic resonance imaging
MRS	magnetic resonance spectroscopy
MRSI	magnetic resonance spectroscopic imaging
NAA	N-acetylaspartate
NAAG	N-acetylaspartylglutamate
NAD	nicotinamide adenine dinucleotide
NADP	nicotinamide adenine dinucleotide phosphate
NMR	nuclear magnetic resonance
NOE	nuclear Overhauser effect
OVS	outer volume suppression
PAG	phosphate activated glutaminase
PC	Pyruvate carboxylase reaction
PCA	portocaval anastomosis
PCho	phosphocholine
PCr	phosphocreatine
PE	phosphoethanolamine
PET	positron emission tomography
PDH	pyruvate dehydrogenase complex reaction
Pi	inorganic phosphate
RF	radio-frequency
SNR	signal-to-noise ratio
Tau	taurine
TCA	tricarboxylic acid cycle
TE	echo time
TR	repetition time
VOI	volume of interest
WS	water suppression

spectra; glutamate and glutamine in ^{1}H and ^{13}C spectra). Moreover, all these spectra were acquired using different acquisition parameters and setups, and consequently their processing/quantification will be different as will be described below. ^{1}H MRS enables the direct detection of an important number of markers of energy metabolism (lactate, glucose, alanine, phosphocreatine, creatine) and neurotransmitters (glutamate, aspartate, glycine, γ-aminobutyrate, N-acetylaspartylglutamic acid). ^{31}P MRS provides information about energetically important metabolites as the three phosphates of adenosine triphosphate (ATP), phosphocreatine (PCr), inorganic phosphate (Pi) and some chemical reaction rates between them. ^{13}C and ^{15}N MRS together with infusions of isotopically labeled substrates can be used to monitor the flow of the isotope of interest into different metabolic intermediates that will appear in the spectrum. ^{13}C MRS offers the possibility to study non-invasively the fluxes through the tricarboxylic acid cycle and glutamine-glutamate cycle *in vivo*. ^{15}N MRS is an alternative approach to ^{13}C MRS to study glutamate-glutamine metabolism. Finally, ^{17}O MRS is also used to measure energy metabolism and is presented in a separate review within this special issue.

A large number of central nervous system pathological states can be characterized using MRS, e.g. brain tumors, demyelinating and neurodegenerative diseases, epilepsy, acute stroke, brain ischemia, infectious brain lesions as well as neonatal and pediatric disorders (hypoxia-ischemia, inherited metabolic diseases, and traumatic brain injury) [2]. The focus of the present review will be on some acquired hyperammonemic disorders [3,4] and on the usefulness of MRS (^{1}H, ^{13}C, ^{15}N and ^{31}P) to investigate *in vivo* some of the molecular mechanisms involved in this type of disease in animal models.

Hyperammonemia (HA) can lead to hepatic encephalopathy (HE), a neuropsychiatric disorder that frequently accompanies severe liver disease (acute or chronic). Increasing evidence points to high blood and brain ammonia concentrations together with its metabolic product, glutamine, as key factors involved in the pathogenesis of HE [3,5–19]. Normally, ammonia is maintained at low levels by the liver (kidney and muscles can also contribute [20]), as excess ammonia is toxic to central nervous system [11,16]. Cerebral ammonia removal relies on formation of glutamine by glutamine synthetase (GS) in astrocytes [14] (unique astrocytic expression of GS [6,21]), leading to astrocytes swelling and brain edema in hyperammonemic cases. Despite important amount of research in the field, the precise mechanisms and their relative contributions to the chronological events leading to astrocytes swelling, brain edema and neurological alterations are very complex and not yet fully elucidated. These mechanisms are only beginning nowadays to be understood. Studies, performed mainly on animal models (*in vivo* or *ex vivo*) or in cell cultures, showed that the main pathogenic mechanisms involved in HE are: amino acids disturbances (i.e. glutamine increase); alterations in neurotransmission/neurotransmitters (i.e. glutamate, γ-aminobutyrate changes); cerebral energy disturbance (i.e. ATP, creatine, phosphocreatine, lactate modifications); alteration of nitric oxide synthesis and oxidative stress which leads to induction of the mitochondrial permeability transition; impairment of axonal and dendritic growth during brain development; signaling transduction pathways; alterations in channels and transporters activity [8,11,14,20,22–25].

To date, MRS (mainly ^{1}H MRS) was successfully used *in vivo* to investigate and monitor acquired hyperammonemic disorders in humans and animal models [3,7,22,26–39]. The main finding of

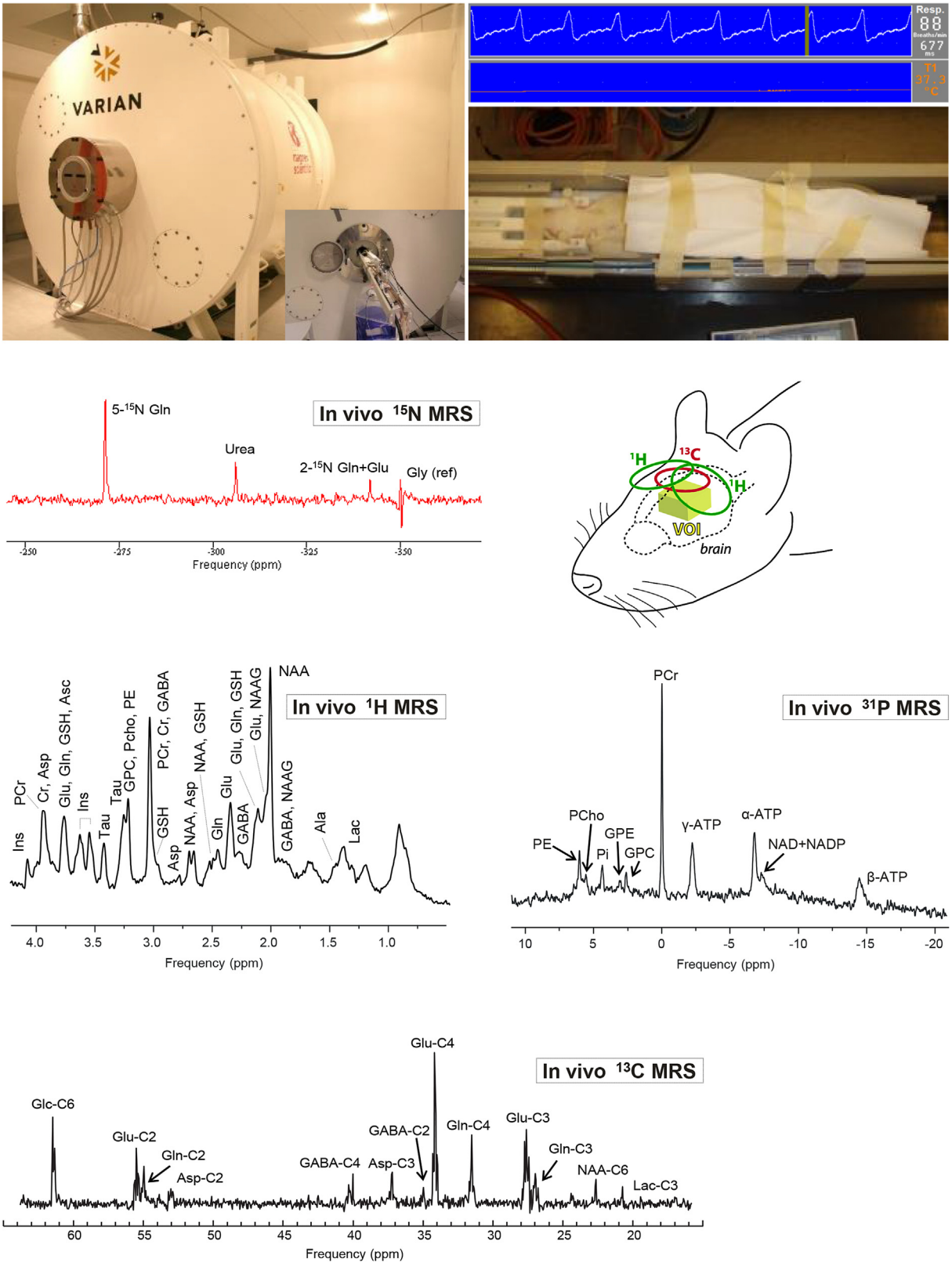

Fig. 1. Setup of an *in vivo* experiment under anesthesia: 9.4T horizontal magnet, animal stereotaxically fixed in a home built holder and monitoring of animal physiology (respiration and temperature using a small animal monitor system, SA Instruments, NY, USA). The placement of the RF coil (i.e. $^{1}H-^{13}C$ coil) and VOI on the rat brain is shown on the drawing in the center of the image. Representative *in vivo* ^{1}H, ^{13}C, ^{15}N and ^{31}P spectra acquired in rat brain at 9.4T under anesthesia.

these studies was the increase in brain glutamine concentration. Glutamine increase can be easily monitored using ^{1}H MRS while changes in energy metabolism and glutamate-glutamine cycle can be investigated using ^{13}C, ^{31}P and ^{15}N MRS.

2. *In vivo* proton Magnetic Resonance Spectroscopy

In vivo Proton Magnetic Resonance Spectroscopy (^{1}H MRS) is one of the most used techniques and a powerful tool to non-invasively investigate *in vivo* brain metabolism of animals and humans in different neurological disorders [2,34]. The hydrogen nucleus (a proton) is the most sensitive nucleus in terms of intrinsic sensitivity (high gyromagnetic ratio (γ)) and high natural abundance (>99.9%) leading to unrivalled signal-to-noise ratio (SNR). As a consequence, compared with other MRS nuclei (^{13}C, ^{15}N, ^{17}O), ^{1}H detection is easy to achieve (within minutes) with no need of infusing labeled substrates to increase SNR.

In vivo ^{1}H MR spectroscopy mainly focuses on carbon-bound protons in the 1–5 ppm range of the chemical shift scale. It can detect low molecular weight metabolites that are present at high enough concentrations (effective proton concentrations of ~0.5 mmol/kg of wet weight (kg_{ww}) or greater, in normal brain or following increases with disease) and mobile on the MR spectroscopic time scale. Since nearly all metabolites contain hydrogens, a large number of biological relevant metabolites can be identified and quantified (with a typical precision of ~10%) *in vivo*.

Nowadays, about 19 brain metabolites can be quantified *in vivo* from a selected volume of interest (VOI) located in the animal or human brain when using high magnetic fields ($B_0 \geq 7$ T) and short echo times (TE < 10–20 ms). These brain metabolites form the so-called neurochemical profile, and are the following: glutamate (Glu), glutamine (Gln), aspartate (Asp), γ-aminobutyrate (GABA), glycine (Gly) (neurotransmitters and associated metabolites); glucose (Glc), lactate (Lac), creatine (Cr), phosphocreatine (PCr), alanine (Ala) (markers of energy metabolism); taurine (Tau), myo-inositol (Ins) (markers of osmoregulation); phosphocholine (PCho), glycerophosphocholine (GPC), phosphoethanolamine (PE), N-acetylaspartate (NAA), N-acetylaspartylglutamate (NAAG) (markers of myelination/cell proliferation) and ascorbate (Asc), glutathione (GSH) (antioxidants). In addition to these metabolites, the macromolecules contributions can also be assessed *in vivo* at high field [40]. However, brain ammonia is not measurable. In the present review we will focus on the measurement of Gln, Glu and some metabolites involved in energy metabolism (i.e. Lac, Cr, and PCr). More details on the role of these metabolites can be found in the review by V. Rackayova in this special issue and in Refs. [34,41,42].

While in high resolution nuclear MR (NMR) the principal goal is to identify unknown compounds and to analyze their structure, for localized *in vivo* MRS the main goal is the reliable detection and subsequent quantification of the concentration (or changes in concentrations) of as many known metabolites as possible in a well-defined region of the brain.

Quantification is challenging and represents the key to successful usage of MRS *in vivo*. Accurate and precise quantification of brain metabolites depends on:

1) Spectral quality and amount of biological information, which is strongly influenced by: hardware performances (such as magnetic field strength, shim and radio-frequency (RF) system), pulse sequence designs and calibrations (e.g. TE, repetition time (TR), localization and outer volume signal suppression (OVS), water suppression (WS), chemical shift displacement error, spectral baseline, RF pulse calibration). An example of *in vivo* ^{1}H MRS spectrum acquired in the rat brain is provided in Fig. 2 showing the main features of good spectral quality.

An important factor affecting the spectral quality is the sensitivity of the nucleus under investigation. Sensitivity (i.e. SNR) increases not only with increasing B_0 field strength but also depends on the performances of radio-frequency coils (see review by Dr O. Ipek in this special issue). As previously shown, high magnetic field strength leads to several main advantages for MRS: increased chemical shift dispersion (spectral resolution), decreased strong coupling effects and higher SNR [43–49]. An example of increased chemical shift dispersion with increasing the magnetic field is shown in Ref. [50] by simulating under *in vivo* conditions Glu and Gln at 1.5T, 4T and 7T. The authors showed a clear separation of Glu and Gln resonances at 2.35 and 2.45 ppm when increasing magnetic field strength to 7T. All these advantages are expected to increase the number of quantifiable metabolites by improving the quantification precision and accuracy for low concentration metabolites, strongly overlapped metabolites and for metabolites having complex multiplet patterns [43–46,51,52]. For example, at 1.5T up to five-six metabolites can be reliably quantified: total NAA (tNAA), i.e. NAA + NAAG, total choline (tCho), i.e. PCho + GPC, total creatine (tCr), i.e. Cr + PCr, at practically all echo-times, Lac at 144 ms echo-time and Ins, Glx (Glu + Gln) if short echo times are used ($\leq$20–25ms) [53–55]. At 3T additional metabolites are measured at short echo-time (i.e. GABA, GSH) and sometimes Glu and Gln can be measured separately [43,46]. When using an even stronger magnetic field ($\geq$7T), up to 19 metabolites can be quantified [2,43,44,46,47,51].

It has to be emphasized that neither a high nor a low magnetic field will automatically guarantee accurate and reliable determination of metabolite concentrations. The spectral quality (i.e. high quality artifact-free spectra) generated with the chosen pulse sequence and parameters is crucial. A large number of details regarding the spectral quality in ^{1}H MRS are provided in the review by Dr L. Xin within this special issue, while the sources and forms of artifacts in *in vivo* ^{1}H MRS spectra have been reviewed in detail elsewhere [56]. Therefore, we will just briefly mention some of the points affecting the spectral quality.

A key factor that influences spectral quality is the adjustment of B_0 homogeneity in the selected VOI (called B_0 shimming or just shimming). If B_0 is spatially inhomogeneous, the resonance frequency of ^{1}H nuclei is not the same over the measured volume of tissue, resulting in broadened spectral lines, in decreased spectral resolution and signal-to-noise ratio. Local B_0 inhomogeneities are mostly caused by susceptibility differences between tissue, air, bone and blood. They are scaled with B_0 and become highly non-linear at high fields leading to increased peak linewidths (in Hz). An adjustment of the B_0 homogeneity for ^{1}H MRS is technically challenging in rodent brain due to the small size of the brain, and optimal B_0 corrections (shims) are necessary [57–61]. More details on B_0 shimming are provided in the review by Dr C. Juchem (in this special issue).

The localization efficiency of the acquisition sequence can be defined as the ability to provide a maximum signal from a selected volume with minimum contamination from outside. This is typically achieved by using strong crusher gradients which eliminate all the unwanted signals. In the 0.5–2 ppm region the subcutaneous lipids represent the main source of contamination. Their presence, typically as phase distorted signals, leads to unreliable concentrations for metabolites present in this spectral region (e.g. Lac, Ala, GABA). This contamination can be limited by the use of additional OVS bands [49,62], which are typically implemented before the localization module. The efficiency of the localization sequence depends also on the chemical shift displacement artifact, representing the spatial displacement of volumes selected for off-resonance signals (e.g. NAA and Cr) relative to the nominal VOI. This is a general issue when using slice-selective pulses for localization (a

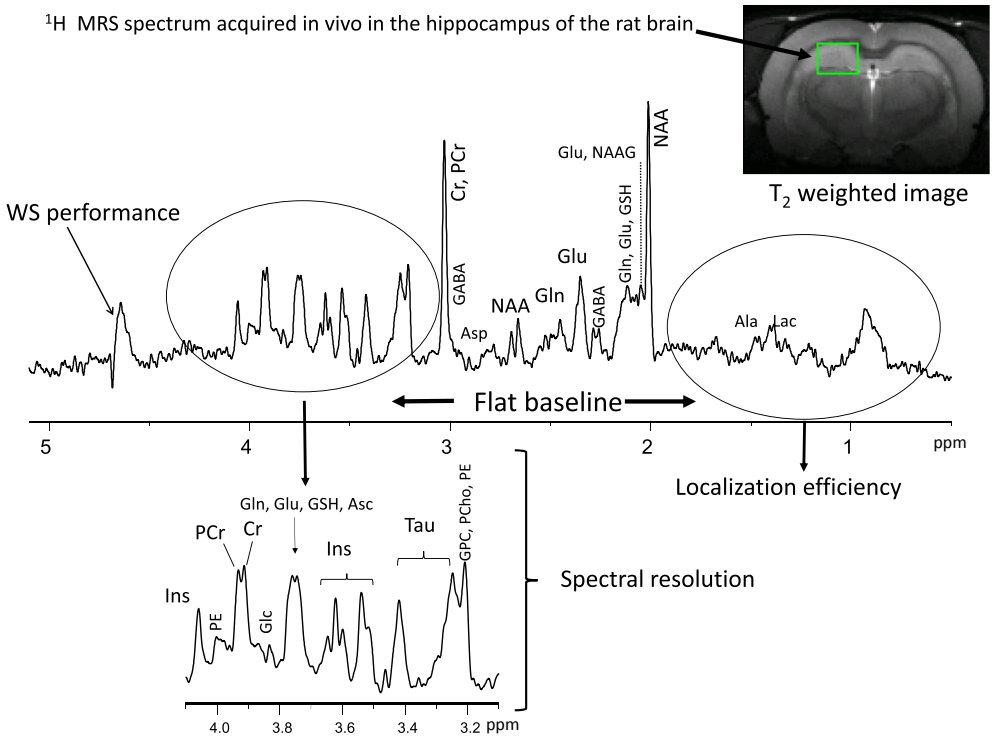

Fig. 2. Representative *in vivo* ^{1}H MRS spectrum acquired in the hippocampus of a rat brain (VOI = 2 × 2.8 × 2 mm^3) at 9.4T using the SPECIAL sequence (TE = 2.8 ms). The main features of a good quality spectrum are shown in the figure (i.e. water suppression (WS), baseline, localization efficiency (no subcutaneous lipid contamination from outside the brain), spectral resolution).

frequency selective RF pulse applied simultaneously with a magnetic field gradient) and becomes significant at high magnetic fields due to increased chemical shift dispersion (i.e. the chemical shift difference between NAA (2.02 ppm) and Cr (3 ppm) is ~1 ppm, which represents 127 Hz at 3T, 300 Hz at 7T and 600 Hz at 14T). This artifact can be limited by using stronger magnetic field gradients; however, attention has to be paid to eddy current effects on the B_0 stability.

Brain tissue contains around 70–80% of water, therefore water represents the dominating peak in the proton signal. Water protons resonate at 4.65 ppm and if unsuppressed, this signal overlaps almost all important metabolite peaks. However, poor water suppression leads to the presence of residual water signal in the acquired spectrum and affects the spectral baseline. A flat baseline is critical for reliable quantification. Several water suppression techniques were developed and are usually implemented before the localization module (sometimes one RF pulse for water suppression can also be used during the localization module to further suppress the partially recovered water signal due to longitudinal relaxation) [63].

The number of quantifiable metabolites can be increased by using short TE, leading to high quality spectra with resolved lines of many metabolites (singlets and coupled resonances are in pure absorption mode) due to minimal signal modulation induced by J-coupling of multiplets of coupled spin systems such as Glu, Gln, Ins, Glc, Asp, Ala, GABA, Asc, PE, Gly and Tau [44,62]. The signal loss due to transversal relaxation is reduced and consequently a more precise quantification is expected. One main drawback of short TE spectra is the presence of underlying broad signals of macromolecules. Generally, for an *in vivo* brain ^{1}H MRS spectrum, the low-molecular weight metabolites are superimposed on signals of high-molecular weight macromolecules. Macromolecule contributions at short TE need also to be considered since an error in the macromolecule estimation can lead to substantial errors in the obtained metabolite concentrations [64–67]. Several techniques have been proposed to overcome this issue and were presented in more details elsewhere [40]. A longer echo time could also be used (TE above 20 ms) but the number of spectral lines, which can be used for quantification, will be reduced. This is due to phase distortion of multiplets produced by coupled spin systems and to fast transversal relaxation leading to signal reduction, preventing the observation of small peaks.

2) Reliable data processing (estimate of the signal amplitude or peak area).

Quantification remains difficult and challenging despite all the previously mentioned advantages of high field and short TE acquisitions. Spectra contain information on many metabolites, each with several resonances representing different hydrogen groups in the molecule. Almost all resonant peaks are severely overlapping, despite increased chemical shift dispersion. This, in addition to the low-concentration metabolites, contribution of macromolecules and residual water signal increases the complexity of ^{1}H MR spectra. In addition, any misadjustment/error in the parameters of the pulse sequence will impact the spectral quality leading to unreliable metabolite concentrations [56]. Therefore, sophisticated approaches incorporating extensive or high level prior knowledge are required for reliable data processing. In the majority of the cases, the metabolite resonances are well known as well as their structure. In this context, the estimation of metabolites concentrations is generally done by fitting the measured *in vivo* ^{1}H MRS spectrum to a linear combination of spectra of known individual metabolites (also called the metabolite basis set), which makes the quantification feasible, especially for low concentration metabolites [40,44,46,68–70].

There are basically two ways to obtain the metabolite basis set:

a) Measuring aqueous solutions of pure metabolites. These measurements have to be done under the same conditions as the *in vivo* ones (the same magnetic field, acquisition sequence, timings, temperature, pH). Any change in the acquisition of *in vivo* data has to be taken into account in the basis set by reacquiring the basis set using the new acquisition parameters. This process is time demanding.
b) Quantum mechanics simulations, based on the density-matrix formalism, using published values of spin-spin coupling constants and chemical shifts [41], and the relevant *in vivo* parameters. Quantum mechanics simulations seem to be a faster alternative, but also more flexible and less expensive. More details can be found in the reviews by Dr Gambarota and Dr Starčuk published in this special issue.

The spectral fitting uncertainties are estimated from the Cramér-Rao lower bounds (CRLB) [71–73], which are independent of the quantification algorithm and estimated using the assumption that the set of model functions is correct and complete. This is obviously a simplification.

Many quantification algorithms depend on user input which might lead to additional inaccuracies. Therefore, the choice of the data processing method is very important. Sometimes, spectra require some pre-processing before the actual quantification step, such as correction for first and second order phase, residual water suppression and zero filling. Data filtering should be avoided and used only for visualization.

Frequency and time domain algorithms, based on metabolite basis sets, are currently used for accurate quantification (i.e. QUEST and AQSES from jMRUI software and TARQUIN working in the time domain; LCModel working in the frequency domain; TDFD working in both time and frequency domains; and others) [55,65–67,74–81]. Some details on several quantification algorithms are provided in Ref. [70]. Fig. 3 shows an example of quantification using LCModel and a simulated basis set on an *in vivo* rat brain spectrum acquired at 14.1T.

3) Quantification strategies (conversion into concentration units).

We have seen so far how to estimate the signal amplitude or peak areas of each metabolite in a given spectrum. The signal amplitude or peak area is proportional to the metabolite concentration. Therefore, by using different quantification strategies we can convert it into tissue metabolite concentration (mmol/kg_{ww}).

The easiest way is to report metabolite ratios, but sometimes these ratios could lead to ambiguous interpretations of metabolic changes. Absolute metabolite concentrations can be more valuable for an accurate interpretation of these changes in different neurological diseases. There are two main quantifications strategies:

a) internal concentration reference, where a known metabolite from the acquired spectrum is considered to have the least variations and is fixed at a certain concentration (e.g. tCr at 8 mmol/kg_{ww}). It has to be emphasized that there is no known metabolite whose concentration never changes in the brain. This is particularly true under pathological conditions or during brain development (for more details on tCr changes see review by V. Rackayova in this special issue). Another option is to use the unsuppressed water signal from the same VOI (this signal is acquired immediately before or after the signal of the metabolites from the same VOI) as internal reference. This approach is widely used for *in vivo* ^{1}H MRS [82,83].
b) external concentration reference where a phantom with a known concentration of compound is placed either very close to the object under investigation and within the sensitive area of the coil or is measured in a separate experiment (phantom replacement technique). This last strategy is widely used for ^{13}C and ^{15}N experiments [84,85].

It has to be emphasized that for each technique several corrections need to be done [86]. An important factor to correct for is the differences in relaxation times between the reference and the *in vivo* metabolites. The effects of relaxation are minimized for acquisitions performed at long TR and short TE (fully relaxed spectra). Therefore, these acquisitions are considered to be a good choice for absolute quantification. The longitudinal relaxation times have been shown to increase with magnetic field [87], leading to increased signal saturation for shorter TR. No further increase in longitudinal relaxation times has been observed beyond 9.4T [88].

2.1. ^{1}H MRS in models of hyperammonemia with or without liver failure

As previously mentioned, ^{1}H MRS can be used either as single point measurement (i.e. at a specific time point during disease evolution) or as a longitudinal measurement where the same animal is measured several times during the disease progression. When performed in a longitudinal way, ^{1}H MRS enables the measurement of concentration changes of certain brain metabolites over time (in our case the increase of glutamine over time) and from the linear fit of these time courses some net accumulation fluxes can be estimated.

^{1}H MRS single point or longitudinal measurements without additional fitting of metabolite time courses were performed in different models of hyperammonemia (acute or chronic liver failure and hyperammonemia *per se* without liver failure). Altogether, there are still few *in vivo* ^{1}H MRS studies performed on these animal models to investigate brain metabolism.

For example, brain metabolism was studied in some experimental models of acute liver failure (ALF) (e.g. portocaval anastomosis followed by hepatic artery ligation, galactosamine or carbon tetrachloride administration) [26,30,35,89–91]. These studies reported an increase of brain Gln concentration together with alterations in brain Lac concentration at later stages of the disease and the presence of brain edema. In a rat model of portocaval anastomosis followed by hepatic artery ligation (measurements performed at 7T, using a fairly big voxel, PRESS at TE = 12 ms, concentrations expressed as ratios to Cr) [89] ammonia was identified as being the principal cause of the alterations in brain metabolisms in ALF. The increase of Lac was suggested to be an indicator of brain energy impairment and having a secondary role in the induction of brain edema, after ammonia [89], even though the mechanisms leading to an increase of Lac are not fully understood. In addition, a decrease in Glu/Cr and NAA/Cr (only at coma stages) was also reported. Early work in the field suggested that an interference of ammonia on the malate aspartate shuttle (MAS) could be a possible cause of lactate increase [92]. NADH produced in the cytosol from the glycolysis needs transport of reducing equivalents across the mitochondrial membrane, such as through MAS, in order to be oxidized. Lactate production can also remove NADH from the cytosol and could therefore be an alternative to the MAS.

Few studies were performed in experimental animal models of chronic liver impairment to assess the kinetics of glutamine and other changes in brain osmolytes in combination with brain energy metabolism. Bile duct ligation (BDL) in rats is an accepted model of chronic HE (type C) associated with cirrhosis, portal hypertension

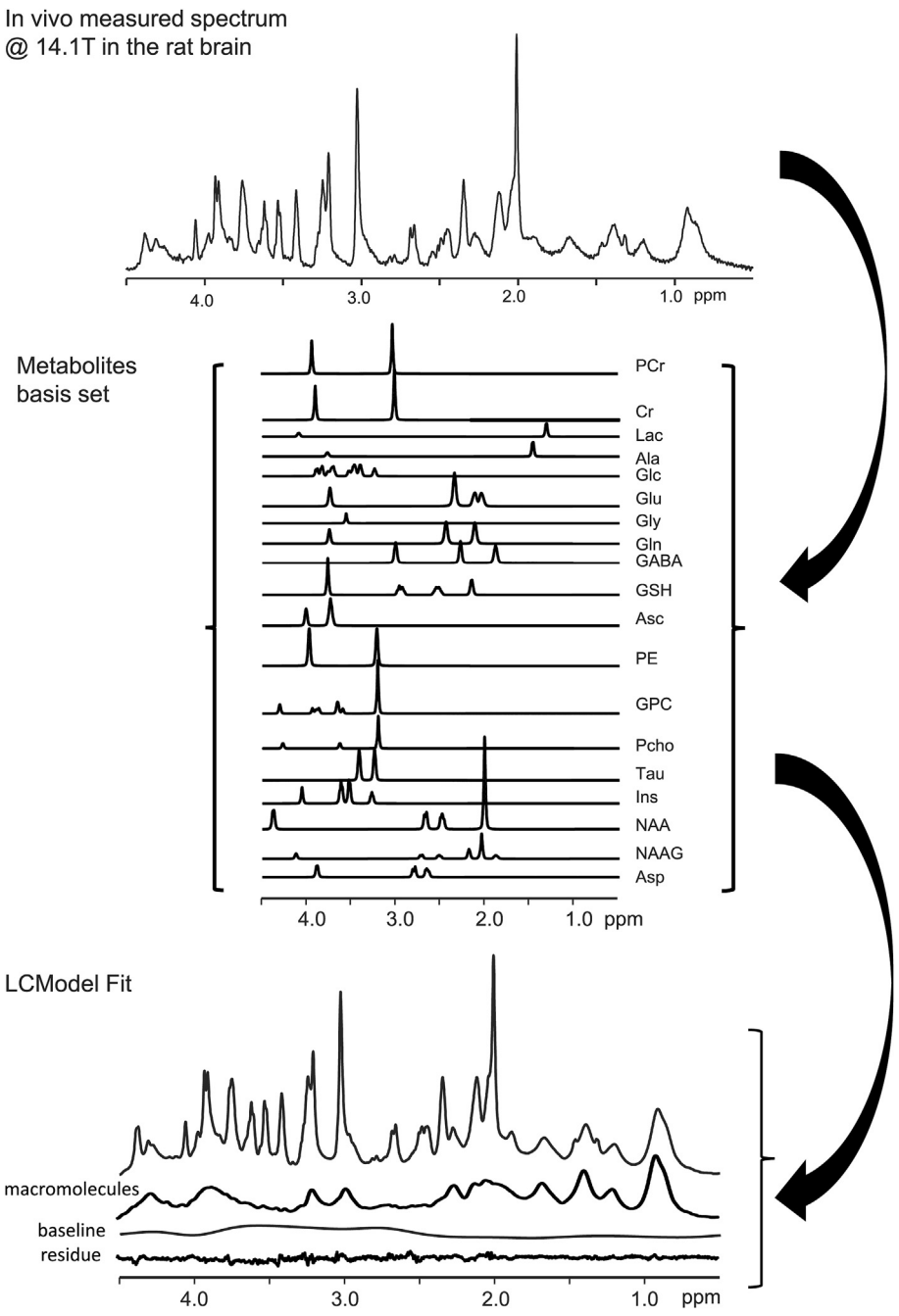

Fig. 3. An example of quantification using LCModel and a simulated basis set on an *in vivo* rat brain spectrum acquired at 14.1T. From top to bottom, the *in vivo* spectrum, the metabolites basis set and the LCModel fit.

and hyperammonemia and is validated by the ISHEN commission [93]. Portocaval anastomosis (PCA) in rats is a popular model to study type B HE and is associated with limited liver dysfunction (liver atrophy and loss of perivenous hepatocytes) and hyperammonemia [93]. The main findings of these studies were increased cerebral glutamine and ammonia levels with sometimes reductions in brain osmolytes reflecting an osmoregulatory response [3,89,94–97]. In a PCA rat model, an additional increase in Lac/Cr was measured while no modifications were found for Glu/Cr and Tau/Cr [89]. BDL rats were studied by two different laboratories using high field ^{1}H MRS [95,97]. Both of these studies were performed in a fairly big VOI with the main difference that a shorter TE was used by Ref. [95] leading to the estimation of an increased number of brain metabolites. Overall the results were similar in both studies showing increase in Gln and decrease in Ins, tCho, Cr, Glu and no significant changes in Lac. It has been proposed that the differences in brain osmolytes could partially explain the different rate of development of brain edema in acute liver failure compared to chronic liver disease [9,98,99].

In order to study the effects of ammonia *per se* without liver failure, some animal models of HA were used (e.g. single i.p. injection of ammonia or continuous infusion for several hours) [27–29,84]. In Ref. [27] single voxel ^{1}H MRS was performed at 7T in cerebellum and substantia nigra (VOI = 3 mm^{3}) after i.p. injection of ammonium acetate using the PRESS sequence (TE = 35 ms). The Gln concentrations were not reported by the authors. A decrease of NAA in cerebellum and an increase of Ins in both investigated brain regions was reported. Ins increase was suggestive of the presence of

vasogenic edema while the NAA decrease was reported to reflect neuronal damage. Using ^{1}H MRS the authors in Ref. [29] showed an increase in Gln during ammonium acetate infusion together with a decrease in Glu concentrations and an increase in Lac concentrations. It was suggested that the increase of Lac was more likely a result of a mismatch between the rate of glycolysis and the activity of tricarboxylic acid cycle (TCA), rather than an attempt by the brain to buffer incoming ammonia.

Our group recently studied the brain metabolism in animal models of HA without liver failure (continuous infusion of ammonium chloride for several hours) and in HA due to chronic liver disease (bile duct ligated rats) in a longitudinal fashion using *in vivo* ^{1}H MRS and MRSI [28,84,95,100]. The objective of these studies were: 1) to follow over time the changes in concentration in as many brain metabolites as possible due to HA by performing our measurements at high field (9.4T) and very short echo time (2.8 ms), an aspect never studied previously; and 2) to acquire additional information on the net glutamine accumulation by fitting the linear increase of glutamine over time (for details on the fitting/modeling please see below in the ^{13}C MRS section).

Using an animal model of HA *per se* and a VOI positioned in a fairly big volume ($5 \times 7 \times 7$ mm^3) placed in the center of the rat brain, we showed that Gln concentration increased immediately after the start of ammonium infusion and continued to increase linearly over time (2.3 ± 0.4 mmol/kg$_{ww}$ before the infusion and 17.7 ± 4.0 mmol/kg$_{ww}$ at the end of the infusion) [84]. This linear and continuous increase of total Gln implies increased anaplerosis [31,101,102], which appears to be coupled to the ammonia detoxification pathway. From the linear fit of Gln increase over time we obtained a net Gln accumulation of 0.033 ± 0.001 mmol/kg$_{ww}$/min, suggesting no delay in Gln accumulation and consequently in anaplerosis. In this model ammonium chloride was continuously infused at 4.5 mmol/h per kilogram body weight for several hours and consequently plasma ammonia concentration increased from 0.08 ± 0.02 mM to 0.95 ± 0.08 mM while brain ammonia concentration was 3.8 ± 0.8 mmol/kg$_{ww}$ at the end of the experiment, in agreement with previous measurements [103–105]. To study the spatial distribution of metabolites in various regions of the brain during ammonium chloride infusion, we further continued our studies using ^{1}H MRSI [28]. Spectra were simultaneously acquired in various brain structures (cortex, hippocampus and thalamus) and metabolic maps were obtained for 5×10 voxels with a nominal voxel size of 1.1 μL for 12 metabolites (i.e. Gln, Glu, Cr, PCr, tCho, Ins, Tau, Lac, NAA + NAAG, PE, Glc, GABA). In this case also the increase in the Gln pool at different time points during infusion was apparent from the maps. The concentrations of all other metabolites remained within 10% fluctuation in standard deviation of the mean concentration over the duration of the experiment. During infusion the Gln increase showed a specific brain region pattern, i.e. higher in cortex than in hippocampus (16.2 ± 2.7 mmol/kg$_{ww}$ in the cortex and 11.5 ± 1.2 mmol/kg$_{ww}$ in the hippocampus), leading to a higher net glutamine accumulation flux in cortex (0.030–0.035 vs 0.025–0.030 μmol/g/min, respectively). The obtained values were in agreement with the measurements performed using single voxel ^{1}H MRS in a big voxel.

We further extended our measurements to the bile duct ligated model [95,100]. For these measurements we used the same methodology as for the HA studies. We showed a gradual increase of Gln reaching 2.5 fold increase at week 8 after BDL. Among the other brain osmolytes only Ins (−36%, weeks 8 vs 0) and tCho (−21%, weeks 8 vs 0) decreased significantly over time. Cr is well known for its roles in energy metabolism and osmoregulation [42,106] and showed a tendency to decrease at week 8 (−11%). These changes suggest a compensatory effect for the osmotic imbalance created by Gln accumulation in agreement with previously published studies in BDL rats and humans [7,32,33,36–38,97]. In addition, the sum of the main osmolytes (Gln, Ins, tCho, Cr) was not constant over time (20% increase). The underlying cause of the observed minimal brain edema associated with chronic HE might therefore be this progressive but incomplete osmotic compensation. Using the combined advantages of ultrashort echo time and a high magnetic field, we detected *in vivo* additional metabolites in this model of HE. For example, the neurotransmitters Glu and Asp showed a significant decrease at week 8 (~20%). No significant changes where measured for the metabolites involved in energy metabolism and for NAA. We further analyzed the correlations between brain Gln, plasma ammonium and brain energy metabolites, to better understand the molecular mechanisms underlying the neurological changes. Plasma ammonium showed the strongest correlations with plasma bilirubin and brain Gln, suggesting that Gln is probably the first brain metabolite influenced by increased blood ammonium. Subsequently, the change in brain Gln showed strong correlations with changes in other brain metabolites (i.e. Ins, Glu, ADP).

Since both models were analyzed in our laboratory using the same methodology, we were able to directly compare the cerebral metabolic pathways involved in the pathogenesis of both diseases. It has to be emphasized that the differences in the neurochemical profile between HA and chronic liver disease (CLD) are clearly visible in the spectra presented in Fig. 4. Even though Gln increased in both cases, the decrease in the brain osmolytes was present only in CLD. Additionally, in CLD glutamine increased similarly in all brain regions [100], contrary to HA where we measured a higher increase of Gln in the cortex [28]. For CLD a long term elevation of brain glutamine may be partially compensated by a decrease in other brain osmolytes, while in HA the fast and short term increase of glutamine does not enable the activation of compensatory mechanisms.

3. *In vivo* carbon Magnetic Resonance Spectroscopy

Carbon is an element which enters the composition of a large number of molecules constituting living tissue, including carbohydrates, proteins, lipids and nucleic acids. Its electronic structure with 4 outer shell valence electrons makes it a key building block for the backbone chemical chain of these molecules, but also for its versatility to create single and double bonds with hydrogen, oxygen, nitrogen and also sulfur and phosphorus. It can generate a large range of chemical geometries, from linear molecules to branch chains and carbon rings. It is therefore an essential atom in life, not only to generate new molecules necessary in tissue growth and repair but plays a central role in the energy supply of living cells, which ends in the production of ATP, the essential cellular energy substrate and CO_2. Mammals consume for this reason a large amount of carbohydrates and fatty acids, which provide the required energy and carbon backbones for many biochemical processes.

The *in vivo* measurement of carbon is therefore of particular interest for the study of the biochemistry of a given organ. Despite this strong biochemical interest, *in vivo* ^{13}C MRS is very far from being as popular as ^{1}H MRS for a series of physical and physiological challenges. Carbon is present in nature as two stable isotopes, ^{12}C and ^{13}C. ^{12}C has a natural abundance of 98.9% and possesses a nucleus made of 6 protons and 6 neutrons, resulting in a zero total nuclear magnetic moment. It is therefore invisible for nuclear magnetic resonance. ^{13}C has an additional neutron in its nucleus, which results in a total nuclear spin ½, similar to the ^{1}H nucleus, and can therefore be used for MRS measurements. The natural distribution of carbon isotopes is not favorable for its detection with MRS, since only 1.1% of the carbons are magnetically active.

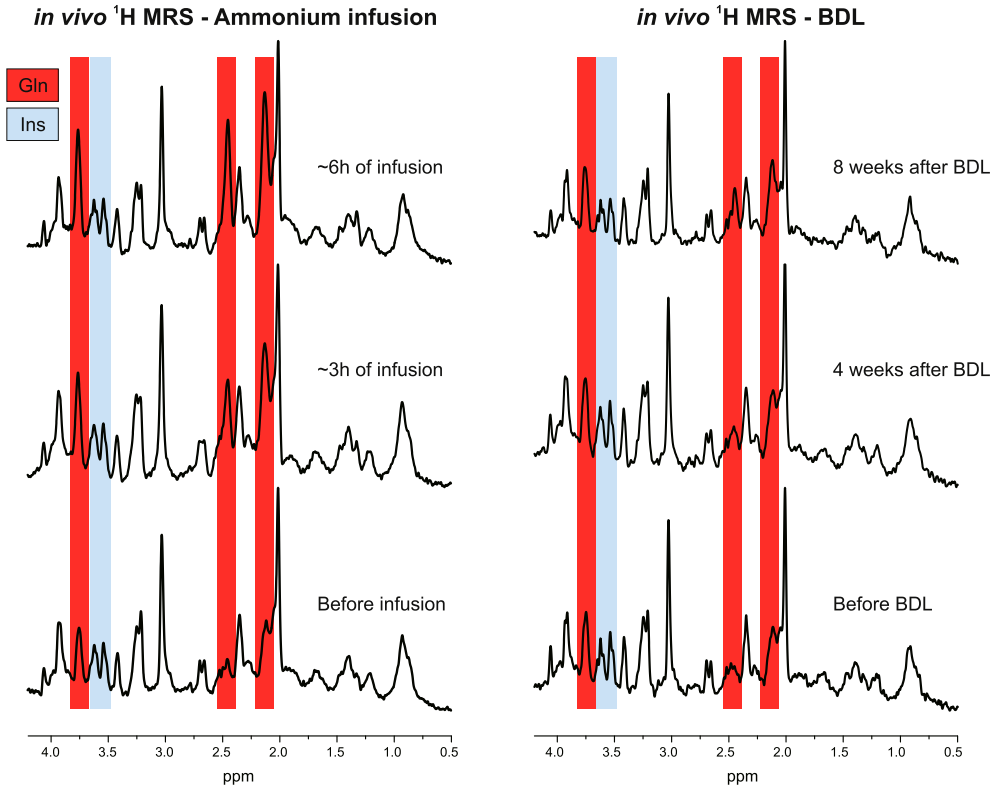

Fig. 4. Representative *in vivo* ^{1}H MRS spectra acquired in the rat brain at 9.4T (TE = 2.8 ms) in two different models: HA *per se* and BDL. In both models, an increase in Gln was measured (Gln peaks highlighted in red: ^{2}CH at 3.8 ppm, $^{4}CH_2$ at 2.4 ppm and $^{3}CH_2$ at 2.1 ppm). A significant decrease in the brain osmolyte Ins (−36%, weeks 8 vs 0) was only observed in the BDL model.

This low natural abundance adds to the intrinsically low sensitivity of NMR detection at body temperature, resulting from the small Zeeman energy splitting between the two nuclear spin states in an external magnetic field as compared to the thermal energy (see review by Dr V. Mlynarik in the present issue). Moreover, the 4 times smaller gyromagnetic ratio of ^{13}C nucleus compared to ^{1}H reduces its coupling with the RF electromagnetic field and its sensitivity of detection. Natural abundance ^{13}C MRS is therefore rarely used as an alternative to ^{1}H to detect metabolites concentrations *in vivo*.

However, the low natural abundance of ^{13}C can be turned into an asset, since ^{13}C can be used for tracer experiments, similar to radionuclides studies. *In vivo* ^{13}C MRS studies are thus typically coupled to an intravenous infusion of a ^{13}C-labeled metabolic substrate. This enables the dynamic measurement of the transit of ^{13}C across the different biochemical pathways involved in the metabolism of the infused substrate in the organ of interest, which carries temporal information on the corresponding chemical reaction rates. As such, it gives ^{13}C MRS the possibilities to probe information on brain metabolism which is not accessible with ^{1}H MRS. Despite the additional physiological difficulties linked with the substrate infusion and plasma level monitoring through blood sampling as well as the high cost of ^{13}C-labeled substrates in the quantity needed for such applications, the unique possibility of ^{13}C MRS to probe brain metabolism *in vivo* with low invasiveness raised strong interest in the field of brain energy metabolism [107] (and reviews by Dr J. Valette and M. Lai in this special issue).

3.1. Brain metabolic pathways involving ^{13}C

The brain meets its energetic demands at rest and during activation largely, if not exclusively by oxidative combustion of fuels. Although glucose is the main energy substrate in cerebral metabolism, other energy substrates are metabolized in the brain, such as acetate and ketone bodies [108], which are sometimes used as alternative ^{13}C tracers. The energy substrates used by the brain are taken up from the blood circulation through the blood-brain barrier by specific transporters, classified as glucose transporters (GLUTs) [109] and monocarboxylate transporters (MCTs) [110]. Although the major part of the endothelial cells are covered by glial endfeet, it remains unclear in what proportion glucose is taken up by glial cells and by neurons [111,112] and whether neurons could be only fueled with pyruvate from the glial cells through the Lac shuttle [108]. After its transport through the blood-brain barrier, glucose is further metabolized to CO_2 and water through the glycolysis and the TCA cycle (Fig. 5), generating high-energy phosphates such as ATP [108].

The glycolysis is the initial step of glucose metabolism and converts the 6-carbon chain of glucose into two molecules of pyruvate (3-carbon chain). When glucose utilization is higher than the oxidative metabolism (TCA cycle rate), non-oxidative metabolism occurs by a net production of Lac from pyruvate. In addition, glucose can be stored in the form of glycogen in astrocytes as an energy buffer which can be converted back to glucose through the glycogen phosphorylation [113].

3.1.1. The TCA cycle

To complete the oxidation of glucose to CO_2, pyruvate enters the TCA cycle via the pyruvate dehydrogenase complex reaction (PDH) [108]. The TCA cycle in the mitochondria not only generates energy-rich molecules in the form of ATP, but also provides precursors for the biosynthesis of compounds including amino acids, in particular glutamate, directly involved in the neurotransmission process. Fig. 6 shows the different molecules and chemical reactions

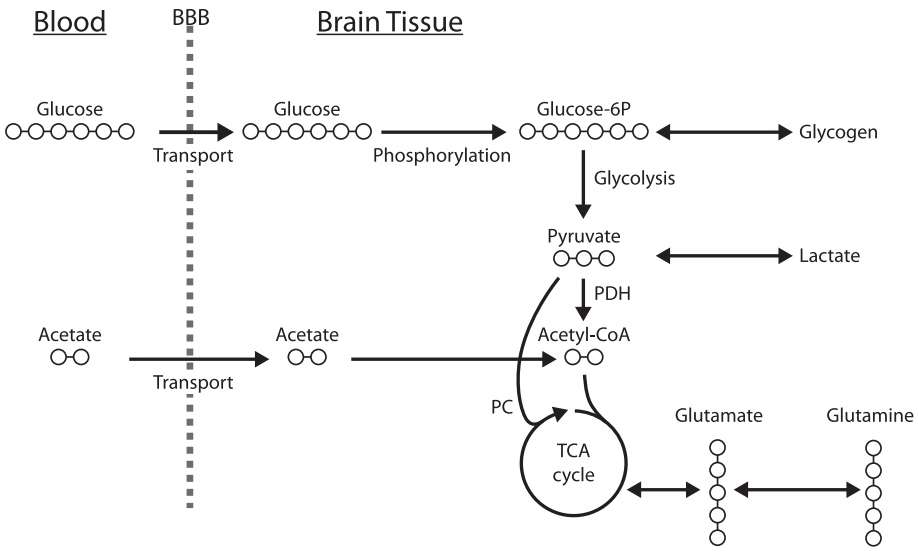

Fig. 5. Schematic view of the main biochemical steps involved in brain energy metabolism. This scheme focuses on the metabolism of glucose and acetate. After transport across the blood-brain barrier (BBB), glucose is phosphorylated and its six carbon chain enters the glycolysis, resulting in the production of pyruvate. Pyruvate carbon backbone enters the TCA cycle either through the pyruvate dehydrogenase pathway (PDH) or through the anaplerotic pyruvate carboxylase pathway (PC) in glial cells. Acetate is transported specifically in glial cells and enters the TCA cycle directly at the level of acetyl-CoA.

involved in the TCA cycle. Pyruvate enters both the glial and neuronal TCA cycle, while acetate is specifically metabolized in the glia [114]. The TCA cycle intermediates are in exchange with the cytosolic amino acids glutamate and aspartate. These exchanges are mediated by aspartate transaminase, glutamate dehydrogenase and the transport across the mitochondrial membrane [108,115].

[1,6–$^{13}C_2$] glucose is a widely used NMR tracer to probe mitochondrial metabolism in rodents. After transport across the blood brain barrier, two molecules of [3–^{13}C] pyruvate are generated from one molecule of labeled glucose through the glycolysis. When infusing [1–^{13}C] glucose, only one molecule of [3–^{13}C] pyruvate is produced, while the second pyruvate molecule generated by the glycolysis is unlabeled.

^{13}C from [1,6–$^{13}C_2$] glucose enters both astrocytic and neuronal TCA cycles at the position C4 of citrate. In the first turn of the TCA cycle, ^{13}C reaches the position C4 of 2-oxoglutarate, which exchanges label with cytosolic glutamate. This transmitochondrial label exchange transfers ^{13}C from the carbon position C4 of 2-oxoglutarate to the position C4 of glutamate.

Due to the symmetry of the succinate molecule, the second turn of the TCA cycle transfers half of the labeled carbons of the position C4 of 2-oxoglutarate to the position C3 of 2-oxoglutarate and the other half to the position C2 of 2-oxoglutarate. Through the transmitochondrial exchange + transamination, [3–^{13}C] glutamate is formed from [3–^{13}C] 2-oxoglutarate.

In the third turn of the TCA cycle, half of the labeled carbons of the position C3 of 2-oxoglutarate reaches the position C2 of the same molecule, while the other half remains at the position C3. At the same time, ^{13}C from the position C2 of 2-oxoglutarate is transferred to the position C1, labeling further the position C1 of glutamate. The position C1 of glutamate is usually not simultaneously measurable with the positions C4, C3 and C2 using ^{13}C MRS, due to the large chemical shift of the C1 carbon position compared to the other resonances [116].

Some reactions are specific to a certain cell type. Pyruvate carboxylase reaction (PC) takes place only in the glial compartment and is the main anaplerotic enzyme [117], generating new intermediates in the TCA cycle at the level of oxaloacetate, which can be further used to generate new glutamate molecules. PC transfers ^{13}C from [3–^{13}C] pyruvate to the position C2 of oxaloacetate, which further labels the position C2 of 2-oxoglutarate and glial glutamate (see Fig. 6). On the other hand, this reaction transfers unlabeled ^{12}C to the position C3 of glial glutamate. This glial specific dilution effect makes it possible to distinguish glial and neuronal TCA cycle activities from glutamate and glutamine ^{13}C time courses following [1,6–$^{13}C_2$] glucose infusion. Moreover, the glial acetyl-CoA, at the entrance of the TCA cycle, is diluted by alternative energetic fuels that glial cells can metabolize, like acetate and fatty acids [118,119].

3.1.2. *The glutamate/glutamine cycle*

The glutamate/glutamine cycle is a major biochemical pathway *in vivo*, directly involved in the glutamatergic neurotransmission process [108,120]. This glutamate recycling process is the result of highly compartmentalized enzymes. Glutamine synthetase is located essentially in astrocytes [121], while the glutamate to glutamine conversion through phosphate activated glutaminase (PAG) is mostly present in neurons [122]. Most of the glutamate is in the neurons, while glutamine is essentially located in the glial cells [123]. Both glutamine and glutamate are 5-carbon chains differing by an amino group at the carbon position 5 of glutamine. In the glutamate/glutamine cycle, the carbon positions are maintained, which means that a carbon located at the position C4 of glutamate will reach the position C4 of glutamine and vice versa.

When using ^{13}C enriched substrates, the result of these neuroenergetic processes is a progressive labeling of the carbon positions of glutamate and glutamine, which are present in the brain in sufficiently high concentrations to be observed with ^{13}C MRS. The dynamics of their labeling contains information on the activity of the glial and neuronal TCA cycles and on the neurotransmission cycle. The total concentration of ^{13}C at a certain carbon position is given by the total intensity of the corresponding ^{13}C resonance, independently of its multiplet structure.

In an *in vivo* experiment, the plasma ^{13}C-glucose fractional enrichment is quickly elevated to a high level of about 50–70% and maintained at this value through continuous intravenous infusion. This input function of labeled substrate is also continuously monitored by arterial blood sampling. The interpretation of the ^{13}C turnover curves of glutamate, glutamine and aspartate in brain tissue from the localized ^{13}C MRS is typically undertaken using a two-compartment model, as presented in Fig. 7, which represents a

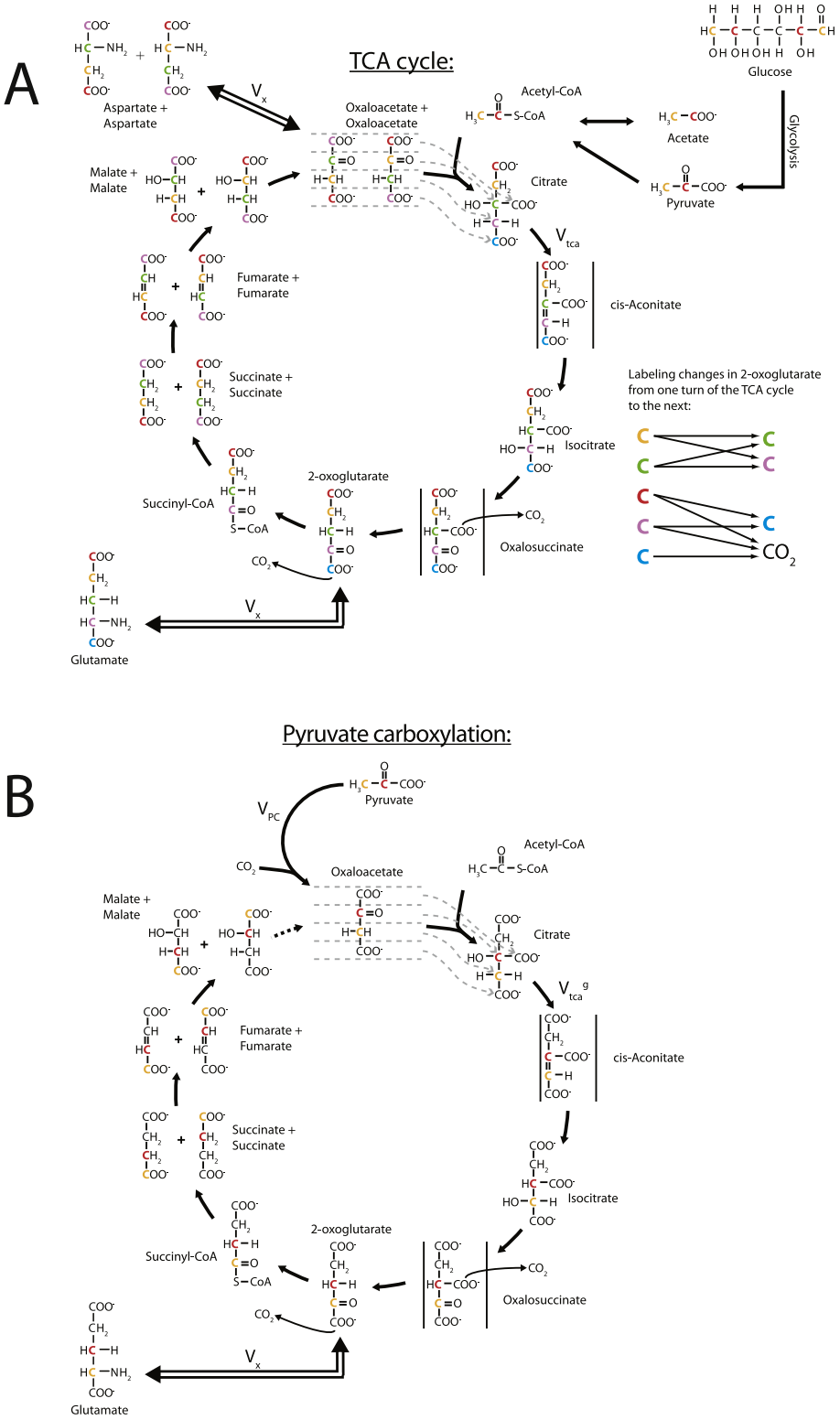

Fig. 6. A) Schematic view of the carbon labeling flow through the TCA cycle. Some parts of the cycle are cell-specific: in the neurons, acetate is not metabolized. The colors enable the follow-up of the carbons from one molecule to the next. The arrows on the right show how carbons are moving in the carbon chain of 2-oxoglutarate from one TCA cycle turn to the next. The carbon positions of glutamate are identical to those of 2-oxoglutarate. In each TCA cycle, the carbons 4 and 5 of citrate are added from acetyl-CoA, while two carbons are lost in CO_2 at the level of oxalosuccinate and 2-oxoglutarate. B) Schematic view of the carbon labeling from pyruvate through pyruvate carboxylation in the astrocytic TCA cycle.

simplified description of the biochemical reactions involved in glucose metabolism. This kind of modeling approach assumes constant metabolic fluxes (noted as V_i) in μmol/g/min and constant metabolic pool sizes, which can be assessed from a ^{1}H MRS acquisition in the same brain location (metabolic steady-state condition). As discussed later, the model can be extended to

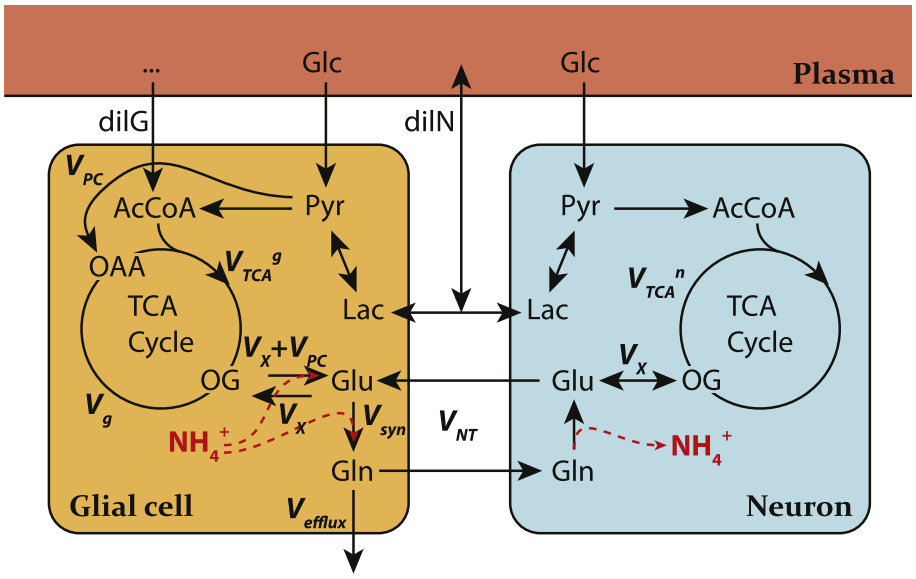

Fig. 7. Model of compartmentalized brain metabolism adapted from Gruetter et al. [115]. Pyruvate (Pyr) originated from glucose consumption is in fast equilibrium with Lac that is exchanged between neurons and glia and is diluted with extra-cerebral Lac through dilN. $V_{TCA}{}^{n}$ is the neuronal TCA cycle, $V_g + V_{PC}$ is the total glial TCA cycle $V_{TCA}{}^{g}$, V_{PC} is the rate of pyruvate carboxylase. In the glial compartment, the dilution of label at the level of acetyl-CoA (AcCoA) by glial specific substrates is accounted by dilG. TCA cycle intermediates oxaloacetate (OAA) and 2-oxoglutarate (OG) exchange with amino acids through the exchange flux V_X. The apparent glutamatergic neurotransmission (i.e. glutamate-glutamine cycle) is V_{NT} and glutamine synthetase rate is V_{syn}. Finally, efflux of labeling from the metabolic system occurs through the rate of glial glutamine loss V_{efflux}. The superscripts g and n distinguish metabolic fluxes in the glial and neuronal compartments, respectively.

include time-varying pool sizes, as necessary for Gln in HA. Under these conditions, the model in Fig. 7 translates into a set of linear differential equations, whose solutions are adjusted to the experimental ^{13}C turnover curves by varying the metabolic fluxes. As a result, the experiment provides a set of metabolic rates and dilution constants ($V_{tca}{}^{g}$, $V_{tca}{}^{n}$, V_x, V_{PC}, V_{NT}, V_{syn}, V_{efflux}, dilG and dilN), which characterize the dynamics of brain glucose metabolism. A detailed description of these modeling processes is given in the review by M. Lai et al. in this special issue.

3.2. Brain metabolic processes involving ammonia

Although the relationship between cause and effect leading to hepatic encephalopathy and the related spectrum of neurological disorders remains unclear, the increased blood ammonia concentration seems to be the central initiating event. Cerebral metabolism of ammonia involves in particular two biochemical reactions able to assimilate ammonia in brain tissue and therefore to decrease its concentration and related toxicity. Those reactions are glutamate dehydrogenase and glutamine synthetase (Fig. 7). Cooper and coauthors [124] showed using L-methionine-S,R-Sulfoximine (MSO), a potent glutamine synthetase inhibitor, in [^{13}N] ammonia infused rats that glutamine synthetase is the major reaction for ammonia detoxification in brain tissue and that without this reaction, the brain is unable to trap efficiently blood-borne ammonia with alternative pathways. Both glutamate dehydrogenase and glutamine synthetase are essentially astrocytic reactions [122,125]. Astrocytes have therefore a central role in ammonia fixation but are simultaneously the principal target of ammonia neurotoxicity. The observation on the secondary role played by glutamate dehydrogenase as compared to glutamine synthetase activity and the specific ^{13}N labeling pattern of glutamine, glutamate and aspartate went against the earlier theories depicting the high depletion of the astrocytic TCA cycle intermediates through glutamate dehydrogenase as the cause of an energy metabolism impairment and insufficient ATP production [14,126] as the main origin of its neurotoxicity.

The exact biochemical reaction changes that generate the accumulation of glutamine in brain tissue also remain only partially understood. Glutamine is a 5-carbon chain that originates from glutamate in the astrocytes and used as precursor for the neuronal glutamate, through the glutamate/glutamine cycle. An increase of glutamine could result from a change in the glutamate/glutamine ratio in this metabolic cycle, the large pool of glutamate being depleted. However, the steady increase of glutamine measured with ^{1}H MRS in HA and CLD models showed simultaneously a significantly smaller decrease in glutamate concentration [84,95,127]. The glial and/or neuronal glutamate pools are therefore replenished accordingly. Since neurons cannot replenish their glutamate pool through anaplerotic processes, the new carbon chains are therefore expected to be provided by astrocytic pyruvate carboxylase and subsequent exchange between 2-oxoglutarate in the TCA cycle and astrocytic glutamate, further converted to glutamine. This process is active in the healthy brain to compensate for carbon chain losses, essentially through glutamine efflux from brain tissue [128] (Fig. 7). The need for new glutamate molecules in the astrocytic compartment as precursor for ammonia fixation through glutamine synthesis requires therefore modified input fluxes in the astrocytic TCA cycle, in particular modifications in the pyruvate carboxylase anaplerotic reaction, which might impact glial oxidative metabolism. Most glutamine is stored in the astrocytic compartment in healthy conditions. An important question that remains unanswered is the exact reaction changes that create the increase in total glutamine concentration. It could be an increase in glutamine synthetase activity because the enzyme is not saturated with NH_3 in the normal brain and its *in vivo* activity increases with increased ammonia concentration in hyperammonemia [105], a decrease in glutamine transfer to neurons or a decrease in glutamine efflux from brain tissue, or any combination of those processes. Since all of these metabolic pathways involve an exchange of carbon chains, ^{13}C MRS is expected to be particularly useful to explore changes in glutamate/glutamine exchange and the impact of the higher glutamine content on oxidative and non-oxidative energy metabolism, particularly in astrocytes.

3.3. Ex vivo/in vitro experiments

In order to understand the disturbance of the biochemical mechanisms that leads to hepatic encephalopathy and address the issue of glutamine synthesis *per se* in conditions of hyperammonemia, a series of ^{13}C MRS labeling studies were conducted in animal models of liver disease. Zwingmann et al. [129] used a model of ALF in Sprague-Dawley rats by portacaval anastomosis followed by hepatic artery ligation. [1−^{13}C] glucose was used as tracer substrate, injected intraperitoneally as a bolus. The animals were sacrificed 15 min after the bolus injection. Both blood samples and brain samples were analyzed for the ^{13}C concentrations and fractional enrichments (ratio of ^{13}C-labeled molecules over the total molecule concentration) of the substrate and metabolic products through perchloric acid (PCA) extraction approaches, and high resolution NMR measurements of the lyophilized PCA extracts resuspended in D_2O. The fractional enrichment can then be determined by the ratio of the peak areas of both $^{1}H-^{13}C$ satellite signals and the $^{1}H-^{12}C$ signal of the molecule in the ^{1}H NMR spectrum, which was used in that study for Lac and Glc measurements, which were then further used as internal reference to scale the ^{13}C spectra and determine the ^{13}C concentrations and fractional enrichments of the other molecules of interest [129,130]. This enabled the determination of the ^{13}C concentrations and fractional enrichments of several metabolite carbon positions, including the Glu and Gln C2, C3 and C4 resonances, Lac C3 and Ala C3. The ^{13}C labeling pattern of these metabolites is a reflection of the upstream metabolic rates, which gives a footprint of brain metabolism that can be compared to a group of sham rats under same infusion protocol. In particular, this gives information on the relative contribution of the anaplerotic compared with the oxidative pathway (PDH). However, the exact quantification of the relative contribution of the anaplerotic pathway is difficult because the labeling at the position C2 and C3 arises both via PC-mediated entry of pyruvate into the TCA cycle and via PDH, in the second turn of the TCA cycle. Taking the C4 to C2 concentration ratio in glutamate and glutamine as an approximation of the PDH to PC activity ratio, it showed an activation of PC relative to PDH, both in precoma and coma stages of ALF, compared with sham-operated controls. The authors also showed an increased *de novo* synthesis of ^{13}C-labeled glutamine from glucose in encephalopathy compared with sham-operated controls. ^{1}H NMR and ^{13}C NMR results showed that both *de novo* synthesis and total concentrations of lactate and alanine increased in precoma and coma stages of ALF.

Using a 6 weeks BDL rat model of CLD under infusion of uniformly labeled ^{13}C-glucose, Bosoi and co-workers [131] took a similar experimental approach, sacrificing this time the rats 30 min after the ^{13}C-glucose intraperitoneal injection. The [U−^{13}C] pyruvate formed from [U−^{13}C] glucose through PDH is metabolized via 2-oxoglutarate in the TCA cycle to [4,5−^{13}C]-labeled glutamate, whereas [U−^{13}C] pyruvate metabolized through PC results in [1,2,3−^{13}C]-labeled metabolites. [4,5−^{13}C]-labeled glutamate and glutamine was therefore taken as a relative measure of PDH activity and [1,2,3−^{13}C]-labeled glutamate and glutamine for PC activity. This neglects further transit from the C4 and C5 carbons of 2-oxoglutarate to the C3, C2 and C1 positions through multiple TCA cycling.

The results showed a 1.6- and 2.2-fold increase in *de novo* synthesis of Lac and glutamine, respectively, and the flux through PDH (2.3-fold increase) and PC (1.8-fold increase) was higher in BDL vs. SHAM rats. From these observations, ammonia-induced increase in brain Lac was interpreted not as a result of energy failure, but rather that the increase in Lac synthesis may occur as a compensatory mechanism to maintain ATP levels [131]. The technique was used further in combination with ^{31}P and ^{1}H NMR to focus on the particular impact of ammonia toxicity under hyponatremic conditions in astrocytes, using astrocyte cell cultures incubated with [1−^{13}C] glucose with or without NH_4Cl [132], from which the authors showed an imperfect correlation of changes in astrocytic glutamine, other organic osmolytes, and the cellular energy state under hyperammonemic stress in isoosmotic and hypoosmotic media, suggesting that additional mechanisms related with astrocyte dysfunction in hyperammonemic states are independent from glutamine formation.

However, those *ex vivo/in vitro* studies could not show a direct link between the increased brain glutamine concentrations or the magnitude of the increase in *de novo* glutamine synthesis rate with the severity of encephalopathy or occurrence of brain edema [133]. ^{13}C NMR studies on brain extracts or cell cultures provided key elements on the metabolic pathways affected by the hyperammonemic conditions to understand HE. However, they suffer from some technical limitations that could potentially hide subtle characteristic changes in TCA cycle activity and glutamate/glutamine cycling as the cause or consequence of hyperammonemia induced HE mechanisms. A first limitation is the measurement at a single time point after the ^{13}C-labeled substrate injection. This limits the analysis to a subset of metabolic flux ratios, under assumptions such as the negligible labeling of the observed carbon positions through the second and third TCA cycle turn. Moreover, since PDH is more active in neurons than astrocytes [134,135], but PC is only present in astrocytes, the time at which the animal is sacrificed might affect the relative balance between the glutamate and glutamine carbon positions labeled through PDH and PC. Other technical limitations are linked to possible post-mortem metabolism during extraction, especially important considering the generation of Lac, as well as possible brain regional differences in the metabolism which are averaged out during the whole brain PCA extraction.

A possibility to overcome this limitation is the use of *in vivo* ^{13}C MRS [107,136–138]. With this approach, ^{13}C NMR spectra are acquired directly *in vivo*, in a localized position in the brain, during the infusion of the ^{13}C-labeled substrate with a temporal resolution of 5–10 min. This non-invasive study of brain energy metabolism enables the measurement of the ^{13}C turnover curves of the carbon labeling positions in the different metabolites, carrying kinetic information on the metabolic rates involved in the TCA cycle and glutamatergic neurotransmission processes. This dynamic information enables one to distinguish between astrocytic and neuronal metabolism and is expected to give further insights into the link between hepatic encephalopathy and changes in metabolism of glutamate and glutamine.

3.4. In vivo ^{13}C MRS

In vivo ^{13}C MRS spectra of brain amino acids show a large chemical shift dispersion as compared to ^{1}H MRS, on the order of 30 ppm range from glutamate C2 to glutamine C3 (Fig. 1). Localized ^{13}C MRS in the brain ensures a proper suppression of ^{13}C signal from extracranial lipids, resulting in a spectrum with a very flat baseline and well separated resonances. The use of the currently available very high magnetic field scanners enables an enhancement of the ^{13}C polarization and related sensitivity of detection, as well as a better spectral resolution, enabling the cleaner separation of the carbon multiplet resonances of neighboring carbon resonances, in particular the C2 of glutamate and glutamine [139]. This is a particular advantage for the spectral quantification of the different carbon resonances, in terms of absolute concentrations. On the flip side, the large frequency range in which the resonances of interest are distributed is a challenge on the transmission side of the MRS experiment, since very large bandwidth pulses are

required to excite or refocus all the resonances in a single repetition cycle. This implies the use of short pulses and therefore strong applied B_1 transmission field, requiring both efficient transmit coils and RF amplifiers. For this reason, most of the *in vivo* ^{13}C MRS studies in the brain were achieved using surface coils, which are well-suited to generate high B_1 fields in a limited tissue space (see the review by M. Lai et al. in this special issue for more details).

The spectrum in Fig. 1 shows the labeling pattern obtained after 4 hours of infusion of doubly labeled [1,6–$^{13}C_2$]glucose. The spectral region between 20 and 65 ppm is of particular interest for the study of oxidative metabolism and neurotransmitter exchange. The C6 resonance of glucose, the infused substrate, is the leftmost resonance, while Lac C3, the result of non-oxidative metabolism of pyruvate C3 is present at 21 ppm. In between the two, the C4, C3 and C2 resonances of glutamate and glutamine are prominent, Aspartate C3 and C2 as well as the GABA resonances C2, and C4 and NAA C3 and C6 are also detectable. The ^{13}C–^{1}H J-coupling effect is frequently cancelled by applying ^{1}H decoupling during the ^{13}C detection, merging that way all the heteronuclear multiplet splitting of each carbon resonance. This spectrum illustrates also the typical ^{13}C–^{13}C J-coupling splitting of the resonances taking place when two neighboring carbons are labeled in the same molecule. This is for example visible on the Glu C4 peak, where the singlet peak is surrounded by the two doublet peaks resulting from the C4–C3 coupling in glutamate, with a shift of 34.9 Hz. The reader is referred to [139] for description of the spectral quantification of ^{13}C MRS data. The reviews by Lai et al. and Valette et al. in the current issue will inform the interested reader with further details on the different aspects of ^{13}C MRS for rodent and human applications.

3.5. Modeling of brain metabolism in ^{13}C MRS studies

In contrast with radionuclide labeling studies such as PET studies, ^{13}C MRS can be used to determine in which molecule and even in which carbon position the ^{13}C atom is incorporated, which is referred to as chemical specificity. These interesting properties of ^{13}C MRS labeling studies raised a strong interest in the neuroscience community in the last decades, providing a deep insight in brain energy metabolism *in vivo*. Early studies were essentially undertaken by infusion of [1–^{13}C] glucose [140–143] and were analyzed with a one-compartment model of brain metabolism. With the rapid improvements of MRS sensitivity and NMR methodology in general, the detection of the carbon positions C4 and C3 of glutamate and glutamine became possible [140], and two-compartment models describing both the glial and neuronal oxidative metabolism and the glutamatergic neurotransmission process were developed [115,144].

The two compartment model is based on the fact that brain tissue is composed of two major cell types, the neurons and the glial cells. They have distinct properties and functions, which rely on their mutual interaction. Neurons are highly specialized cells responsible for processing and transmission of information through electrochemical signals in the central nervous system. Glial cells are responsible to support and protect the neurons in the brain, but are also an active part of the neurotransmission process through the uptake of the neurotransmitter glutamate from the synaptic cleft [145] and play a role in synaptic plasticity [146].

3.5.1. Mathematical modeling of non-steady-state metabolic conditions

In hyperammonemic models, the equilibrium concentrations are modified over time through the neuroprotective actions of specific ammonia-fixing pathways, in particular glutamine synthesis in the astrocytes [144]. This induces a progressive change in the total concentrations of glutamine, resulting in a progressive decrease of the glutamate to glutamine ratio. In the metabolic modeling of ^{13}C-glucose infusion experiments, metabolic steady-state is typically assumed over the period of the MRS data acquisition, which means that metabolic fluxes and total metabolite concentrations are assumed to be constant over this period [107]. If this is a conservative assumption in healthy subjects, this condition might prove to be wrong under hyperammonemic conditions, since a significant change of glutamine and possibly glutamate happens. However, the impact of those changes must be compared to the timing at which they happen as compared to the experiment duration. In CLD, the glutamine increase is a relatively slow process which happens over weeks, resulting in a typical increase of 1–1.2 μmol/g/week for BDL rat models [95], which can be assumed negligible over a typical ^{13}C MRS experimental time of 4–6 h. On the other hand, in acute hyperammonemia models, with and without liver failure, the changes in glutamine concentration take place with a rate of about 0.033 ± 0.001 μmol/g/min [84], on the same time scale as the ^{13}C infusion experiments. Therefore, this non-metabolic steady-state condition has to be taken into account. *In vivo* ^{1}H MRS studies showed that glutamine concentration follows a linear increase from 2.3 ± 0.4 μmol/g before the infusion to 17.7 ± 4.0 μmol/g at the end of the infusion [31,84]. Mathematical models of brain energy metabolism are characterized by two sets of equations, the mass-balance equation and the labeling equations (see Ref. [107] and M. Lai et al. in the present issue). The labeling equations handle the ^{13}C transfer in itself between molecules, while mass-balance equations deal with the total concentrations of those molecules, also known as pool size. The increase of glutamine has therefore to be included in those equations. A standard mass balance equation for a product P with i influxes and j outfluxes is given by:

$$\frac{dP(t)}{dt} = \sum_i V_{in}^i - \sum_j V_{out}^j$$

In the metabolic steady-state conditions, this is equal to zero, which fixes the relation between the sum of influxes and outfluxes. In the case of a time-varying pool size, the net change needs to be included in the modeling. In the hyperammonemic situation, a robust way of doing this is to characterize the increase in glutamine by ^{1}H MRS in the same brain location as the ^{13}C MRS acquisition. Since glutamine concentration rises linearly, the slope of this increase can replace the left term in the mass-balance equation of glutamine and fix the new relation between the fluxes. This gives the following equation for glutamine in the two-compartment model (Fig. 7):

$$\left[\frac{d[Gln(t)]}{dt}\right]_{\substack{measured\ with \\ H_1\ MRS}} = V_{syn} - V_{efflux} - V_{NT}$$

Using the ^{1}H MRS measurement as input does not generate additional degrees of freedom in the mathematical fitting of the turnover curves, which in turn ensures a stability of the metabolic modeling comparable to the normoammonemic conditions. The increase of glutamine concentration can be either determined prior to the start of the ^{13}C infusion study or followed throughout the ^{13}C MRS measurements, for example by using ^{1}H-[^{13}C] MRS approaches [147]. A similar approach was used by our group for the modeling of brain metabolism under infusion of sodium [2–^{13}C] acetate in rats, which resulted in slow time-varying concentrations of glutamate and glutamine [135].

4. *In vivo* nitrogen Magnetic Resonance Spectroscopy

Compared to ^{1}H MRS and ^{13}C MRS, ^{15}N MRS is rather more challenging and therefore not as widely used. This is mainly due to ^{15}N low natural abundance (0.365%) and low intrinsic sensitivity (low gyromagnetic ratio), leading to a low SNR *in vivo*. As for ^{13}C MRS, to overcome these issues, continuous infusions of ^{15}N labeled substrates are used (e.g. ^{15}N labeled ammonium chloride, ammonium acetate). The possibility to monitor the dynamic incorporation of ^{15}N across different molecules involved in important metabolic pathways represents the main advantage of infusing labeled substrates. As previously stated, this information is not accessible when using classical ^{1}H MRS. ^{15}N MRS is an alternative and sometimes complementary approach to ^{13}C MRS in studying glutamate-glutamine metabolism and can in principle provide a more direct interpretation of glutamine metabolism than ^{13}C studies (i.e. ^{15}N label enters directly into the glutamine - glutamate cycle, providing a direct measurement of glutamine synthetase rates (V_{syn})).

Additionally, ^{15}N MRS offers some other advantages. The acquired *in vivo* spectra benefit from a wide chemical shift dispersion leading to the resolution of the important metabolites involved in glutamine-glutamate cycle. As previously published [84,104] the majority of the ^{15}N signals comes from inside the brain. Therefore, there is no need for sophisticated localization sequences. OVS based localization is easy to implement and therefore suitable for these types of applications. Two ^{15}N spectra acquired *in vivo* in the rat brain with and without OVS localization are presented in Fig. 8. By comparing the resonances of [5−^{15}N] Gln from the two spectra, we can notice that almost the entire signal comes from the brain. Moreover, there are no resonances from water or fat present in the spectra which needs to be suppressed and monitored for additional artifacts. To enhance the ^{15}N signal, additional NOE (nuclear Overhauser effect used to transfer magnetization from ^{1}H to ^{15}N nuclei) and ^{1}H decoupling (RF irradiation at the ^{1}H frequency during ^{15}N signal acquisition) modules are implemented in the acquisition sequence [84].

Finally, the ^{15}N spectra are characterized by the presence of very few resonances leading to a straightforward quantification. For example, AMARES (Advanced Method for Accurate, Robust, and Efficient Spectral fitting) [148] from the jMRUI software is an improved interactive time domain algorithm, easy to use with no need of using a metabolite basis set. The prior knowledge is generated by manually selecting the resonances to quantify by clicking on the top of each of them and afterwards defining the linewidth. Then, the prior knowledge is given in terms of relative or fixed amplitudes, frequencies, linewidths, phases and lineshapes (also called low level prior knowledge). The flexibility for the user is increased and therefore any error created by the user can additionally lead to unreliable metabolite quantification. For ^{15}N signals, two Lorentzian spectral components are usually selected to fit the major contributions of the metabolites ([5−^{15}N]Gln and [2−^{15}N] Gln + Glu), the zero-order phase estimated and the first-order phase fixed to zero. The precision of the amplitude estimates is assessed using the CRBs. Absolute quantification is, on the other hand, more challenging and performed using an external reference method [84]. The amplitudes of the localized *in vivo* signals are compared with those obtained under identical experimental conditions from a phantom solution containing ^{15}N uniformly labeled glutamine and glutamate. A small sphere containing a different ^{15}N labeled compound is placed in the center of the ^{15}N coil and used to correct for the effect of variable coil loading on sensitivity between *in vivo* and phantom measurements. In addition, NOE and T_1 effects need to be taken into account by performing each time two different acquisitions: one performed with NOE using the parameters of the *in vivo* experiment and the second using fully relaxed conditions in absence of NOE [84,140].

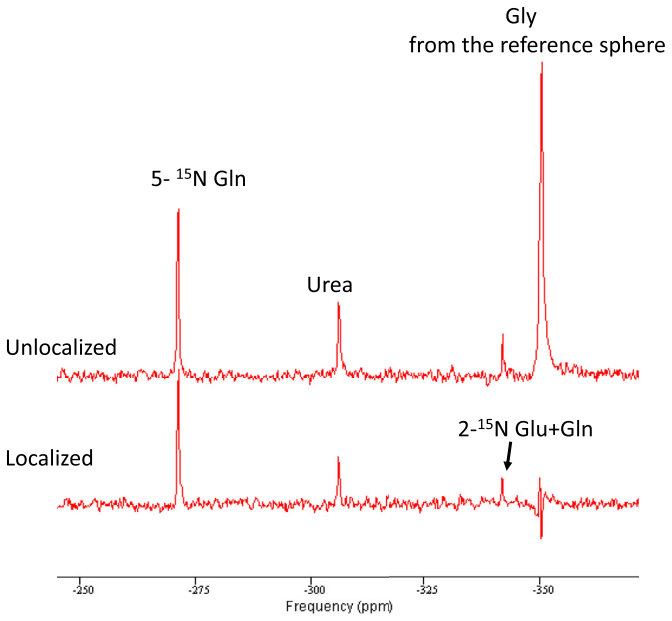

Fig. 8. Representative *in vivo* ^{15}N spectra acquired in the rat brain at 9.4T during ^{15}N labeled ammonium chloride infusion. The labeled urea visible in the spectrum is a consequence of labeled urea release from the liver, distributed across blood circulation to all tissues.

However, an important drawback of ^{15}N MRS *in vivo* experiments has to be mentioned, i.e. the careful monitoring of animal physiology during ^{15}N labeled ammonia infusions. In our laboratory we mainly used ^{15}N labeled ammonium chloride that was infused at a continuous rate of 4.5 mmol/h/kg and a plasma ammonia concentration of 0.95 ± 0.08 mmol/L was reached. The physiological variables were maintained within normal physiology (pH = 7.41 ± 0.04; $PaCO_2$ = 40.0 ± 1.8 mm Hg, O_2 saturation > 99.8%) during the *in vivo* experiments. However, we noticed a tendency of decreasing arterial pH. Therefore, sodium bicarbonate diluted in Dulbecco's Phosphate Buffered Saline was infused continuously at an adjustable rate to maintain arterial pH in the normal physiological range.

A very comprehensive description of ^{15}N MRS is provided by the review of Dr K. Kanamori published in this special issue. In the present review we will focus only on the direct detection of ^{15}N labeled metabolites and on the improvements done in our laboratory from methodological and metabolic modeling point of view [84].

The past *in vivo* MRS studies under ammonia infusion mainly focused on the incorporation of ^{15}N of ammonia into [5−^{15}N]Gln measuring the apparent GS flux (V_{syn}) [31,103–105]. The glutamate dehydrogenase flux (V_{GDH}) was also estimated by measuring [2−^{15}N]Gln + Glu signal during ^{15}N-enriched ammonia infusion in a separate experiment [149]. It is however difficult to determine V_{syn} and V_{GDH} simultaneously in the same subject in an *in vivo* and localized experiment, due to the large chemical shift dispersion between [5−^{15}N]Gln and [2−^{15}N]Gln + Glu.

As for ^{13}C MRS, a two compartment (neurons/glial cells) mathematical model can be used to follow the incorporation of ^{15}N label across different metabolic pathways and to estimate different brain metabolic fluxes related to enzyme activities in the *in vivo* brain. Fig. 7 shows in red the brain metabolic processes involving ammonia in a model of compartmentalized brain metabolism. Ammonia has two components: a gaseous (NH_3) and ionic (NH_4^+)

one, being mostly present as NH_4^+ at physiological pH. Both of them are transportable across cell membranes and thus entering the cells: NH_3 is lipid soluble, entering the brain through diffusion; while NH_4^+ has similar properties as K^+, competing with K^+ on K^+ transporters and channels [150]. The infused ^{15}N labeled ammonia passes the blood-brain-barrier (BBB) and enters directly the glial cells at a rate V_{in}. In astrocytes ammonia and Glu are converted to Gln through GS, leading to the labeling of Gln at the position N5. This labeling can be directly measured in the ^{15}N spectra (Fig. 9) and provides the measure of the flux through GS (V_{syn}). Afterwards, Gln is released by the astrocytes and transported into the neurons where it is converted in Glu by glutaminase, completing the glutamate-glutamine cycle. Ammonia can also be incorporated in glial glutamate through glutamate dehydrogenase leading to labeling of [2−^{15}N]Glu + Gln, which can also be followed directly in the ^{15}N spectra giving the flux V_{GDH} (Fig. 9). Then glutamate is converted into glutamine by GS, which is transported into neurons and converted to glutamate by neuronal glutaminase.

Although the glutamine synthetase reaction is fast in rat brain, Glu/Gln labeling is however a combination of total concentration changes and labeling turnover. The purpose of the study shown in Fig. 9 was therefore to determine over an extended period what the consequences of hyperammonemia are on brain biochemistry of these amino acids, following the change in total brain glutamine concentration. As can be seen from the ^{15}N turnover curves in Fig. 9, the labeling in N5 and N2 reaches rather quickly (<1 h) a dynamic labeling steady-state, in the sense that the ^{15}N concentration in these positions follows then the same linear trend as that of the total Gln or Glu + Gln concentration (keeping the fractional enrichment constant).

More details about the modeling are provided in the review by M. Lai in this special issue. It is well known that a higher number of experimental labeling curves will increase the robustness of the modeling process, the number of estimated parameters and their accuracy. We therefore developed a new alternate acquisition strategy to measure in the same experiment the total glutamine (tGln) accumulation using ^1H MRS and the incorporation of ^{15}N into both [5−^{15}N]Gln and [2−^{15}N]Glu + Gln using ^{15}N MRS, an approach never reported previously. Mathematical modeling of ^1H and ^{15}N MRS data provided reliable estimations of net glutamine accumulation (V_{syn}-V_{nt}), V_{syn}, the apparent neurotransmission rate V_{nt} and V_{GDH} under ^{15}N-labeled ammonia infusion in the rat brain.

[5−^{15}N]Gln and [2−^{15}N]Glu + Gln signals show a large chemical shift difference in ^{15}N spectra (~70 ppm) which makes them difficult to fully excite in a single experiment using conventional acquisition sequences with the carrier frequency placed on the [5−^{15}N]Gln resonance. Therefore, we developed a new ^{15}N pulse sequence starting from the conventional SIRENE sequence [151] to simultaneously detect [5−^{15}N]Gln and [2−^{15}N]Gln + Glu *in vivo* [84]. This was done using two adiabatic excitation pulses with opposite frequency modulations and by acquiring the two ^{15}N signals of interest separately in an interleaved mode. The first adiabatic half passage (AHP) RF pulse with the carrier frequency placed on the [5−^{15}N]Gln fully excites this resonance (no longitudinal (Z) magnetization remaining), but barely affects the Z magnetization of [2−^{15}N]Glu + Gln. After 3 s the second AHP RF pulse with the carrier frequency on [2−^{15}N]Glu + Gln flips the magnetization of [2−^{15}N]Glu + Gln into the transverse plane, whereas the Z magnetization of [5−^{15}N]Gln is slightly reduced by this pulse. This interleaved excitation scheme enables the selective excitation of the two resonances of interest in the same effective TR. The main improvement of this new sequence was the detection of [2−^{15}N] Glu + Gln signal approximately 50 min earlier than with the conventional sequence due to a better RF excitation, which in

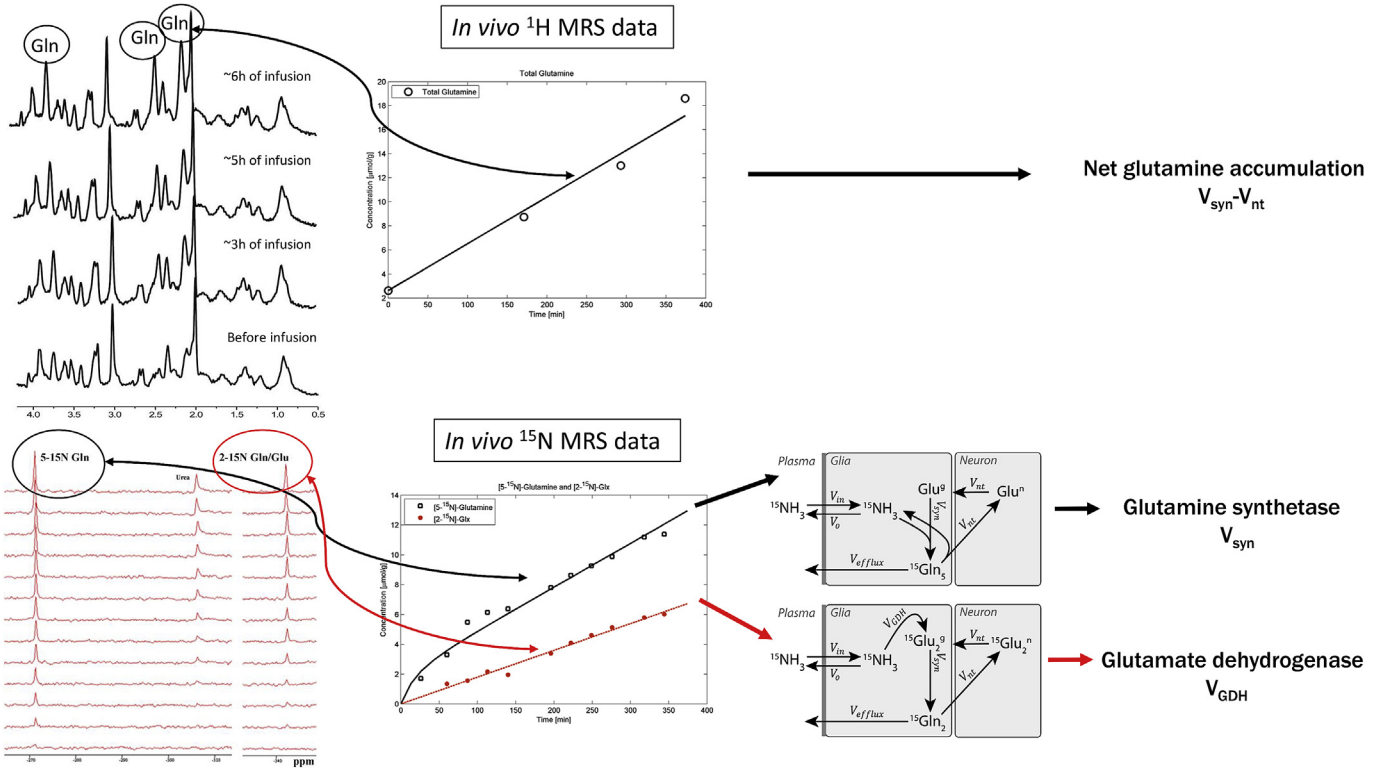

Fig. 9. Representative *in vivo* ^1H and ^{15}N MRS spectra and corresponding time courses obtained during ^{15}N labeled ammonium chloride infusion and used for mathematical modeling. The modeling approach for the ^{15}N data was simplified by merging the glial and neuronal Gln pools into a single kinetic pool, which was shown to have no significant impact on the determined parameters. The Gln kinetic pool is drawn in the glial compartment, which contains 90% of Gln in normal healthy conditions. The arrow to neuronal glutamate represents therefore both Gln transport to the neuron and conversion to Glu in the neuronal compartment.

turns leads to an increased precision for the estimation of V_{GDH} flux.

4.1. Mathematical modeling of ^{1}H and ^{15}N spectra during ammonium chloride infusion

For our experimental setup, the time courses of total Gln (^{1}H MRS measurements), [5−^{15}N]Gln and [2−^{15}N]Glu + Gln (^{15}N MRS measurements) were used as experimental data to which the model was fitted (Fig. 9). The models can be defined using SAAM II environment (The SAAM Institute, Seattle, WA, USA) or in-house Matlab routines using differential equations derived for [Gln], [5−^{15}N]Gln and [2−^{15}N]Glu + Gln.

As mentioned in section 3.5, from a modeling point of view the metabolic system is in non-steady-state conditions since the total Gln concentration is linearly increasing over time during ammonia infusions. The modeling of the time course of total glutamine concentration obtained from the ^{1}H MRS measurement is described at the end of section 3.5 and provided us the measure of the net rate of glutamine accumulation (0.033 ± 0.001 mmol/kg$_{ww}$/min) [84]. The direct measurement of the dynamic labeling of brain ammonia was not possible, therefore V_{in} was assumed 0.23 mmol/kg$_{ww}$/min [20,31,124] together with a negligible efflux from the Gln pool compared to V_{syn} [31,104,105]. Previous measurements of net Gln accumulation [31] were done indirectly by extrapolation and assumed that the increase of glutamine is attributed to increased PC and GDH activities which were considered equal to each other and accounting for the net transport of ammonia. These measurements were confirmed by experimental measurement of Gln accumulation at the end of the *in vivo* experiment.

Following the same metabolic modeling approach as for the interpretation of the kinetic ^{13}C MRS concentration curves (see Ref. [107] and M. Lai et al. in the present issue), the mass-balance equation and the labeling equation of the measured metabolites and their precursors can be written in terms of metabolic fluxes.

In the model presented in Figs. 7 and 9, metabolic steady-state conditions for the fluxes (i.e. constant) and involved chemical pools is assumed, except for glutamine, which increases over time.

4.1.1. Pool sizes considerations

4.1.1.1. Glutamate. The mass-balance equation for total glutamate is then given by:

$$\frac{d[Glu]}{dt} = \frac{d[Glu^{n}]}{dt} + \frac{d[Glu^{g}]}{dt} = V_{nt} - V_{nt} + V_{nt} + V_{GDH} - V_{syn} = V_{nt} + V_{GDH} - V_{syn} = 0 \quad (1)$$

From equation (1) and the metabolic steady-state of glutamate, we obtain the following relation between the fluxes:

$$V_{syn} = V_{nt} + V_{GDH} \quad (2)$$

4.1.1.2. Glutamine. For glutamine, the mass-balance equation is:

$$\frac{d[Gln]}{dt} = V_{syn} - V_{nt} - V_{efflux} \quad (3)$$

Assuming constant metabolic fluxes, glutamine change over time will be characterized by a linear increase:

$$[Gln](t) = [Gln](t=0) + \left(V_{syn} - V_{nt} - V_{efflux}\right)t \quad (4)$$

Which simplifies to:

$$[Gln](t) = [Gln](t=0) + (V_{syn} - V_{nt})t \quad (5)$$

When assuming a negligible V_{efflux} as compared to V_{syn}, as reported by Refs. [31,104,105].

4.1.1.3. Brain ammonia. Assuming metabolic steady-state conditions for the involved fluxes and chemical pools, except for glutamine, brain ammonia is characterized by the following mass-balance equation:

$$\frac{d[NH_3]_{brain}}{dt} = V_{in} + V_{nt} - (V_o + V_{syn} + V_{GDH}) = 0 \quad (6)$$

$$\Rightarrow V_o = V_{in} + V_{nt} - V_{syn} - V_{GDH}$$

4.1.2. ^{15}N labeling dynamics

4.1.2.1. Brain ammonia. Its labeling equation takes into account the fractional enrichment in ^{15}N of each precursor pool as follows:

$$\frac{d^{15}NH_{3\,brain}}{dt} = V_{in}\frac{^{15}NH_{3\,plasma}}{[NH_3]_{plasma}} + V_{nt}\frac{[5-{}^{15}N]Gln}{[Gln]} - (V_o + V_{syn} + V_{GDH})\frac{^{15}NH_{3\,brain}}{[NH_3]_{brain}} \quad (7)$$

The fractional enrichment of ammonia in plasma (FE_{plasma}) is typically assumed to be constant during the infusion period, which is valid and consistent with relatively low ammonia levels before infusion (0.08 ± 0.02 mM). Blood ammonia enrichment follows therefore tightly the injected enrichment. Using the result of equation (6), equation (7) can be rewritten:

$$\frac{d^{15}NH_{3\,brain}}{dt} = V_{in}\,FE_{plasma} + V_{nt}\frac{[5-{}^{15}N]Gln}{[Gln]} - (V_{in} + V_{nt})\frac{^{15}NH_{3\,brain}}{[NH_3]_{brain}} \quad (8)$$

4.1.2.2. [5−^{15}N] glutamine. The labeling of [5−^{15}N] glutamine is thus given by:

$$\frac{d[5-{}^{15}N]Gln}{dt} = V_{syn}\frac{^{15}NH_{3\,brain}}{[NH_3]_{brain}} - V_{nt}\frac{[5-{}^{15}N]Gln}{[Gln]} \quad (9)$$

The first term on the right of equation (9) can be isolated from the labeling equation of brain ammonia (equation (8)). Equation (9) is then rewritten as:

$$\frac{d[5-{}^{15}N]Gln}{dt} = V_{syn}\left(\frac{V_{in}}{(V_{in}+V_{nt})}FE_{plasma} + \frac{V_{nt}}{(V_{in}+V_{nt})}\frac{[5-{}^{15}N]Gln}{[Gln]} - \frac{1}{(V_{in}+V_{nt})}\frac{d^{15}NH_{3\,brain}}{dt}\right) - V_{nt}\frac{[5-{}^{15}N]Gln}{[Gln]} \quad (10)$$

$$\frac{d[5-{}^{15}N]Gln}{dt}+\frac{V_{syn}}{(V_{in}+V_{nt})}\frac{d^{15}NH_{3\,brain}}{dt} = V_{syn}\left(\frac{V_{in}}{(V_{in}+V_{nt})}FE_{plasma}+\frac{V_{nt}}{(V_{in}+V_{nt})}\frac{[5-{}^{15}N]Gln}{[Gln]}\right) - V_{nt}\frac{[5-{}^{15}N]Gln}{[Gln]} \quad (11)$$

Changes in $NH_{3\ brain}$ can be assumed to be small in comparison with the large glutamine pool ("small pool approximation" [152,153]), *i.e.*:

$$\frac{d[5-{}^{15}N]Gln}{dt} \gg \frac{d^{15}NH_{3\,brain}}{dt} \quad (12)$$

Equation (11) is then simplified to:

$$\frac{d[5-{}^{15}N]Gln}{dt} = \frac{V_{syn}V_{in}}{(V_{in}+V_{nt})}FE_{plasma}+\frac{V_{syn}V_{nt}}{(V_{in}+V_{nt})}\frac{[5-{}^{15}N]Gln}{[Gln]} - V_{nt}\frac{[5-{}^{15}N]Gln}{[Gln]} \quad (13)$$

In equation (13), not only the ^{15}N-labeled metabolite concentrations are changing over time, but the total [Gln] concentration is also increasing, as glutamine is in a metabolic non-steady-state condition, as described in the ^{13}C section of this review. Using equation (5), equation (13) can be rewritten more explicitly:

$$\frac{d[5-{}^{15}N]Gln}{dt} = \frac{V_{syn}V_{in}}{(V_{in}+V_{nt})}FE_{plasma} + \frac{V_{syn}V_{nt}}{(V_{in}+V_{nt})}\frac{[5-{}^{15}N]Gln}{[Gln](t=0)+(V_{syn}-V_{nt})t} - V_{nt}\frac{[5-{}^{15}N]Gln}{[Gln](t=0)+(V_{syn}-V_{nt})t} \quad (14)$$

$$\frac{d[5-{}^{15}N]Gln}{dt} = \frac{V_{syn}V_{in}}{(V_{in}+V_{nt})}FE_{plasma} - V_{nt}\left[\frac{(V_{in}+V_{nt})-V_{syn}}{(V_{in}+V_{nt})}\right] \times \frac{[5-{}^{15}N]Gln}{[Gln](t=0)+(V_{syn}-V_{nt})t} \quad (15)$$

From equation (15), the initial slope of the [5−^{15}N]Gln labeling curve can be derived:

$$\lim_{t\to 0}\left(\frac{d[5-{}^{15}N]Gln}{dt}\right)=\frac{V_{syn}V_{in}}{(V_{in}+V_{nt})}FE_{plasma}, \quad \text{since } [5-{}^{15}N]Gln(t=0)=0 \quad (16)$$

4.1.2.3. [2-^{15}N] glutamine and glutamate. From the model in Fig. 9, the rate of labeling of [2−^{15}N]Glu^{g}, [2−^{15}N]Gln and [2−^{15}N] Glu^{n} can be derived:

$$\frac{d[2-{}^{15}N]Glu^{g}}{dt} = V_{GDH}\frac{{}^{15}NH_{3\,brain}}{[NH_3]_{brain}} - V_{syn}\frac{[2-{}^{15}N]Glu^{g}}{[Glu^{g}]} + V_{nt}\frac{[2-{}^{15}N]Glu^{n}}{[Glu^{n}]} \quad (17)$$

$$\frac{d[2-{}^{15}N]Gln}{dt} = V_{syn}\frac{[2-{}^{15}N]Glu^{g}}{[Glu^{g}]} - V_{nt}\frac{[2-{}^{15}N]Gln}{[Gln]} \quad (18)$$

$$\frac{d[2-{}^{15}N]Glu^{n}}{dt} = V_{nt}\frac{[2-{}^{15}N]Gln}{[Gln]} - V_{nt}\frac{[2-{}^{15}N]Glu^{n}}{[Glu^{n}]} \quad (19)$$

Again, the linear increase of [Gln] in hyperammonemia has to be included in the modeling. The "small pool approximation" [152,153] is assumed for $^{15}NH_{3\ brain}$. Using equation (8), the isotopic enrichment of brain ammonia can be isolated and inserted in equation (17):

$$\frac{d[2-{}^{15}N]Glu^{g}}{dt} = V_{GDH}\left(\frac{V_{in}}{(V_{in}+V_{nt})}FE_{plasma} + \frac{V_{nt}}{(V_{in}+V_{nt})}\frac{[5-{}^{15}N]Gln}{[Gln]} - \frac{1}{(V_{in}+V_{nt})}\frac{d^{15}NH_{3\,brain}}{dt}\right) - V_{syn}\frac{[2-{}^{15}N]Glu^{g}}{[Glu^{g}]} + V_{nt}\frac{[2-{}^{15}N]Glu^{n}}{[Glu^{n}]} \quad (20)$$

$$\frac{d[2-{}^{15}N]Glu^{g}}{dt} + V_{GDH}\frac{1}{(V_{in}+V_{nt})}\frac{d^{15}NH_{3\,brain}}{dt} = V_{GDH}\left(\frac{V_{in}}{(V_{in}+V_{nt})}FE_{plasma}+\frac{V_{nt}}{(V_{in}+V_{nt})}\frac{[5-{}^{15}N]Gln}{[Gln]}\right) - V_{syn}\frac{[2-{}^{15}N]Glu^{g}}{[Glu^{g}]} + V_{nt}\frac{[2-{}^{15}N]Glu^{n}}{[Glu^{n}]} \quad (21)$$

The "small pool approximation" is given by the following expression:

$$\frac{d[2-{}^{15}N]Glu^{g}}{dt} \gg \frac{d^{15}NH_{3\,brain}}{dt} \quad (22)$$

Finally, the labeling equation of glial glutamate (equation (17)) can be directly written in terms of plasma ammonia enrichment as:

$$\frac{d[2-{}^{15}N]Glu^{g}}{dt} = V_{GDH}\left(\frac{V_{in}}{(V_{in}+V_{nt})}FE_{plasma} + \frac{V_{nt}}{(V_{in}+V_{nt})}\frac{[5-{}^{15}N]Gln}{[Gln]}\right) - V_{syn}\frac{[2-{}^{15}N]Glu^{g}}{[Glu^{g}]} + V_{nt}\frac{[2-{}^{15}N]Glu^{n}}{[Glu^{n}]} \quad (23)$$

Equations (18), (19) and (23) are a set of three coupled differential equations, also coupled to the [5−^{15}N]Gln enrichment. The sum of the numerical solution of these three equations can then be fitted to the measured [2−^{15}N]Glu + Gln.

5. *In vivo* phosphorus Magnetic Resonance Spectroscopy

In vivo ^{31}P MRS is closer in sensitivity to ^{1}H MRS than to ^{13}C MRS,

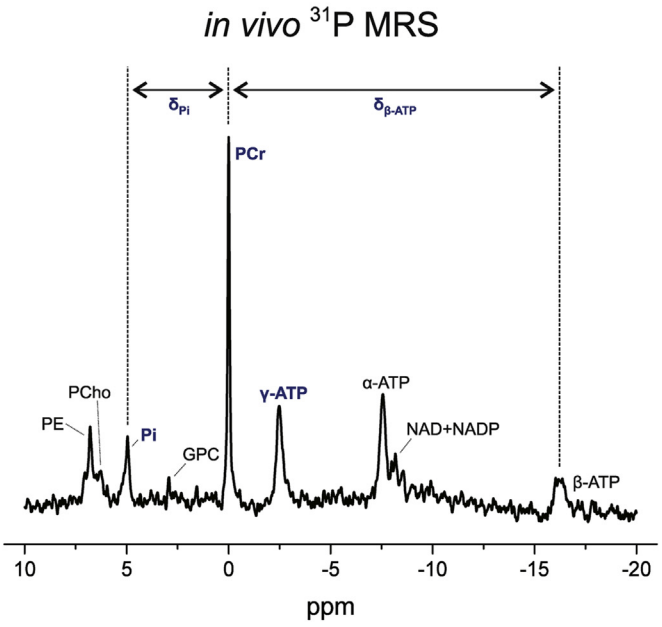

What can be assessed from ^{31}P MRS (in combination with ^{1}H MRS)

Intracellular pH

Calculated based on the difference in resonance frequencies between Pi and PCr signals (δ_{Pi}) in ppm

$pH = 6.75 + \log[(\delta_{Pi} - 3.29)/(5.68 - \delta_{Pi})]$ (1)

Concentration of Mg^{2+}

Assessed from the difference in resonance frequencies between β-ATP and PCr signals ($\delta_{\beta\text{-ATP}}$) in ppm

$pMg^{2+} = 4.24 - \log[(\delta_{\beta\text{-ATP}} + 18.58)^{0.42}/(-15.74 - \delta_{\beta\text{-ATP}})^{0.84}]$ (2)

Concentration of ADP

Calculated using ATP concentration measured by ^{31}P MRS, Cr and PCr concentrations measured by ^{1}H/^{31}P MRS and the value for apparent equilibrium constant of creatine kinase reaction (K_{CK}) from literature (ideally adapted for each particular pH and $[Mg^{2+}]$) (3)

$[ADP] = ([ATP] \times [Cr])/([PCr] \times K_{CK})$

The phosphorylation potential (PP)

Using **ATP** and **Pi** concentrations measured by ^{31}P MRS; ADP concentration calculated above

$PP = [ATP]/([ADP] \times [Pi])$ (4)

Relative rate of ATP biosynthesis ($v/V_{max\text{-}ATP}$)

Using **Pi** concentration measured by ^{31}P MRS; ADP concentration calculated above

$v/V_{max\text{-}ATP} = 1/(1 + 0.2/[ADP] + 0.13/[Pi])$ (4,5)

Relative rate of CK reaction ($v/V_{max\text{-}CK}$)

Using **PCr** concentration measured by ^{1}H/^{31}P MRS; ADP concentration calculated above; with $K_{m\text{-}ADP} = 0.8$mmol/l and $K_{m\text{-}PCr} = 5.0$mmol/l (6)

$v/V_{max\text{-}CK} = ([ADP]/([ADP] + K_{m\text{-}ADP})) \times ([PCr]/([PCr] + K_{m\text{-}PCr}))$ (4)

Fig. 10. Representative localized ^{31}P MRS spectrum acquired *in vivo* in the rat brain at 9.4T (VOI = 4 × 7.5 × 6.5 mm^3, localization using OVS in x and z direction and ISIS in y direction, no decoupling and no NOE) and corresponding calculations. References: (1): [163], (2): [164], (3): [165], (4): [156], (5): [166], (6) [167].

having a 100% natural abundance and no need for infusion of any labeled substrates. The intrinsic ^{31}P sensitivity is however lower, only ~7% MRS sensitivity compared to protons. For animal studies, this translates into the need of longer acquisition times or expansion of the VOI to reach a SNR similar to ^{1}H MRS. As previously mentioned, ^{31}P MRS provides different information on the

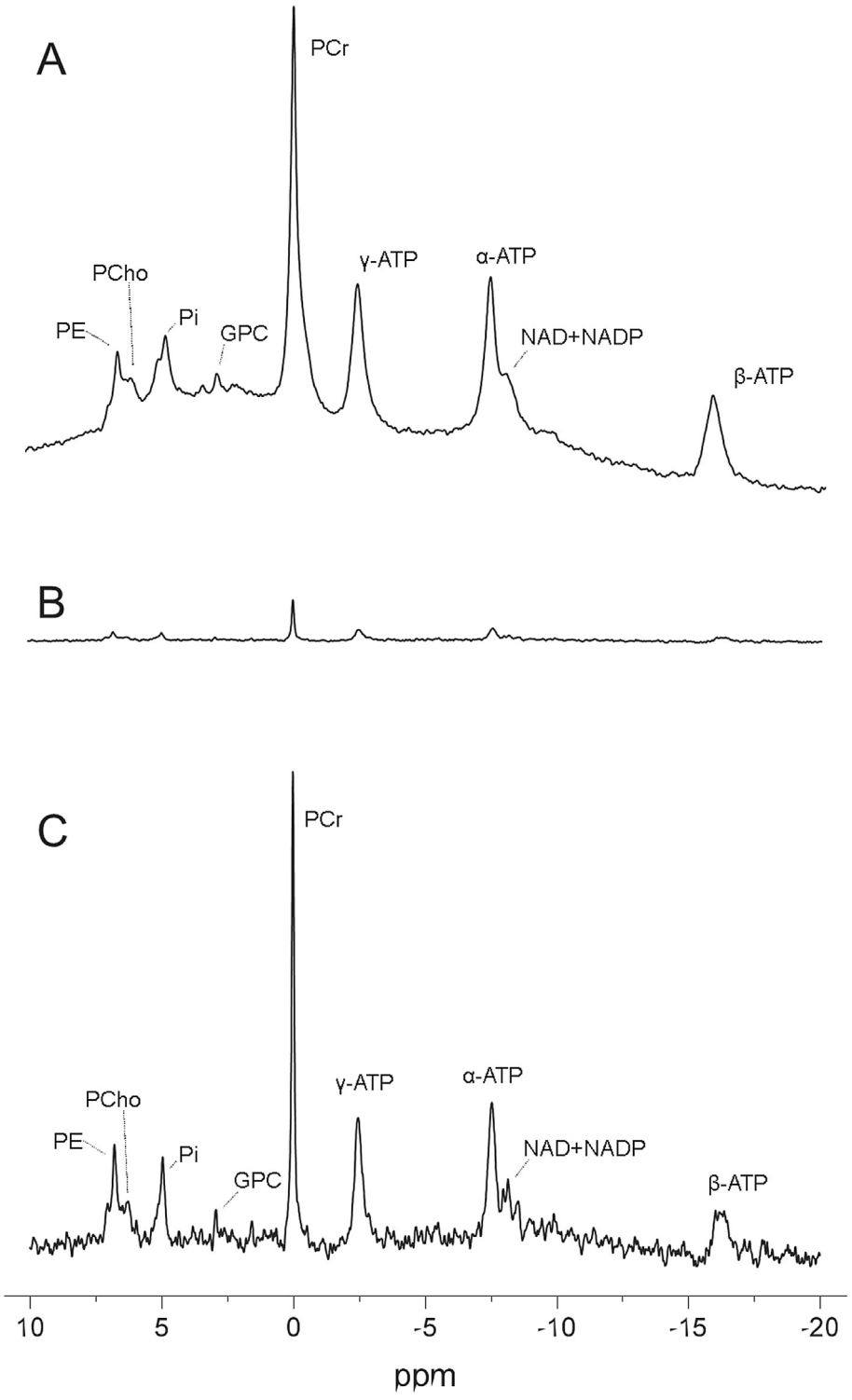

Fig. 11. *In vivo* ^{31}P MRS spectra acquired in the rat brain at 9.4T. A) unlocalized spectrum; B) localized spectrum acquired from the same rat, acquisition parameters and same scaling (VOI = 4 × 7.5 × 6.5 mm^3); C) same spectrum as in B) but at a different scaling.

energetically important metabolites from ^{1}H MRS and therefore it should be considered as a complementary approach to obtain additional information.

The review of Dr L. Valkovic in this present issue gives a general overview of ^{31}P MRS *in vivo*, therefore in this chapter we will focus on brain static ^{31}P MRS in animal models of HA. In addition, the review of V. Rackayova in this special issue provides a description of the roles of Cr/PCr and their measurement by ^{1}H and ^{31}P MRS.

In vivo brain phosphorous spectra contain the contribution of few metabolites with limited number of resonances and a significant chemical shift dispersion (~30 ppm), leading to a better separation of metabolites and easier quantification than ^{1}H MRS. Fig. 10 shows a representative *in vivo* ^{31}P spectrum acquired in the rat brain. The PCr resonance is the most important one and by

convention is fixed to 0 ppm. Other high energy phosphates that can be detected are the three resonances of ATP which originate from the three non-equivalent phosphate groups α, β and γ. Due to homonuclear J-coupling (coupling with adjacent ^{31}P nuclei), α and γ-ATP are doublets whereas β-ATP is a triplet with typical J-coupling constants of ~16 Hz. These multiplets are not always resolved *in vivo*. Pi is another metabolite detected *in vivo* and involved in important chemical reactions of energy metabolism. Brain ^{31}P spectra contain also the contribution of phosphomonoesters and diesters which are cell membrane precursors and cell membrane degradation products, respectively. PCho and PE are the major contributors to the phosphomonoesters signal, while GPC and glycerol-phosphoethanolamine are the main components of the phosphodiesters. The signals of phosphomonoesters and diesters are characterized by an additional heteronuclear scalar coupling (^{31}P–^{1}H) which is in the range of ~6–7 Hz leading to undesirable line broadening. Finally, the resonance of nicotinamide adenine dinucleotide (NAD; doublet) overlapping with the one from nicotinamide adenine dinucleotide phosphate (NADP; doublet of doublet) can also be detected. In addition to the concentration of the visible phosphorus metabolites mentioned above, ^{31}P MRS offers the possibility to calculate some new parameters as shown in Fig. 10. The exact chemical shift position of some resonances is sensitive to intracellular pH and Mg^{2+} concentration. This is due to the fact that protonation (or complexation with magnesium) of a compound changes the chemical environment of neighborhood nuclei leading to a change in their chemical shift. This allows one to calculate the intracellular pH via the chemical shift difference between PCr and Pi using the modified Henderson-Hasselbach equation. The amount of free Mg^{2+} can also be calculated from the chemical shift between PCr and β-ATP (Fig. 10). The two resonances of adenosine diphosphate (ADP) overlap with the resonances of α and γ-ATP, which together with the low *in vivo* concentration makes them difficult to directly detect *in vivo*. As shown in Fig. 10, ADP concentration can however be calculated using ATP, Cr and PCr concentrations due to its involvement in the creatine-kinase reaction. Additionally, the phosphorylation potential, relative rate of ATP biosynthesis and relative rate of creatine-kinase reaction can be estimated using the concentrations of ATP, Pi, ADP, and PCr [95,154–156].

^{31}P MRS spectra need to be acquired using localization modules to eliminate the contaminations originating from cranial musculature and bone phosphate. The cranial musculature mainly contaminates the PCr signal since muscle contains a substantial amount of PCr, while bone phosphate produces an extremely broad resonance leading to a hump-shaped baseline (Fig. 11). The main localization modules used for ^{31}P MRS are ISIS, STEAM, PRESS and SIRENE. To avoid J-coupling evolution and loss of signal due to T_2 relaxation, pulse-acquire sequences are preferred. In our laboratory, we used a combination of OVS (in two directions: x, and z) with an additional 1D ISIS (to localize a slice in y direction) similar to the SIRENE localization. Fig. 11 shows spectra acquired with and without localization modules at the same scale and at different scales optimized for display, all acquired *in vivo* in the same animal at 9.4T. As can be seen, the localized spectrum is characterized by a flat baseline, narrow linewidths but significantly lower SNR. Several options can be used to increase SNR in ^{31}P spectra: broadband ^{1}H decoupling applied during the signal acquisition aims to eliminate the heteronuclear interactions and was used to improve the quantification of phosphomonoesters and diesters; NOE applied during the full TR (using for example low power ^{1}H decoupling) was used to increase the SNR by ~30% (but not for all metabolites); ultrahigh field MR systems lead to an increase in SNR and spectral resolution. Similar to ^{15}N MRS there is no contamination from the water signal in the spectra which would need to be suppressed and monitored for additional artifacts.

In vivo brain ^{31}P spectra are characterized by the presence of a limited number of resonances and a significant chemical shift dispersion leading to a straightforward quantification. As for ^{15}N MRS, AMARES algorithm [148] from the jMRUI software is most often used. Recently, LCModel was also used for ^{31}P MRS quantification together with a simulated basis set [157]. In terms of absolute quantification, as for ^{1}H MRS, different approaches can be used (internal or external concentration reference), with the exception that the water signal cannot be used as internal reference. In place of the water signal, the PCr concentration from ^{1}H MRS can be used. This approach is however more time demanding since one ^{1}H spectrum needs to be acquired separately from the same voxel. In addition PCr is strongly overlapping with Cr and therefore a reliable quantification of the two needs to be achieved first. Very often, ratios to PCr or ATP are presented, assuming that the concentrations of these two compounds are relatively stable. In some diseases this assumption does not apply, for more detail please see the review by V. Rackayova in this special issue.

5.1. ^{31}P MRS in models of hyperammonemia

The pathogenic mechanisms in hyperammonemia-induced HE have been repeatedly associated with disturbances in energy metabolism. However, their direct role is still elusive. In this context ^{31}P MRS is a well suited technique to measure the energy charge by measuring the high energy phosphates. To date there are very few *in vivo* ^{31}P studies performed in animal models of HA and the results are sometimes controversial. For example no changes in ^{31}P metabolites were measured in a model of acute liver failure [35] or in a model of hyperammonemia *per se* [29]. It has been postulated that the discrepancies can be due to the differences in ammonium exposure or severity and timing of clinical symptoms [158]. The majority of the ^{31}P MRS studies performed in CLD were performed in humans and the results are here again quite controversial [159–162].

In a rat model of chronic hepatic encephalopathy (due to chronic liver disease) we performed an *in vivo* and longitudinal study combining high field ^{31}P with ^{1}H MRS [95]. This study revealed mild changes in some energy metabolites: 8 weeks after BDL, rats showed a tendency toward ATP decrease (−10%, $p = 0.07$), a gradual decrease in ADP (−28%, $p = 0.003$) together with a progressive decrease in cerebral pH reaching 0.03 pH decrease at week 8 ($p = 0.002$) and a significant decrease in relative rate of creatine kinase (CK) reaction $v/V_{max\text{-}CK}$ (−18%, $p = 0.012$). Other metabolites measured by ^{31}P MRS did not show any significant change. This decrease in brain ADP, pH and $v/V_{max\text{-}CK}$ was significantly correlated with increase in plasma ammonium. Regarding the fact that all changes in energy metabolites appear mainly late in the progression in the illness, it can be concluded that the perturbation of brain energy metabolism is not a major cause of early symptoms of chronic hepatic encephalopathy in adult brain.

6. Conclusion

MRS has proven to be a promising tool, providing information about metabolite concentration changes and metabolic fluxes which are directly linked to some specific molecular mechanisms. The non-invasive applicability of this technique combined with the unique advantages of high magnetic fields enables, as shown here, the time evolution assessment of changes in certain metabolites.

^{1}H, ^{13}C, ^{15}N, ^{31}P MRS have specific requirements from a methodological point of view and contain different information on brain metabolites. Used in alternative/combined way they are a powerful diagnostic tool and very useful to assess several pathological

mechanisms involved in HE. It is important to emphasize that ALF, CLD and HA *per se* are very different models of HE with increased ammonium and Gln as common factor, therefore leading to MRS results that are different and sometimes controversial. In addition, the extraordinary developments in MRS combined with other *in vivo* MR imaging techniques promise new perspectives for a better understanding of pathogenic mechanisms involved in HE but also for a more reliable diagnostic in HE by establishing precise correlations between different profiles of metabolites and the degrees of HE.

Acknowledgments

Supported by Centre d'Imagerie BioMédicale (CIBM) of the UNIL, UNIGE, HUG, CHUV, EPFL, the Leenaards and Jeantet Foundations, EU Grant FP7-PEOPLE-2012-ITN project 316679 TRANSACT and the Swiss National Science Foundation (SNF grant 3100A0-116859 and 31003A-130278). The authors thank Dr V. McLin (Pediatric Gastroenterology Unit, Department of Child and Adolescent, University Hospitals of Geneva (HUG), Geneva, Switzerland) collaborator on the BDL project briefly presented in the present review and G. Donati (Laboratory for Functional and Metabolic Imaging (LIFMET), Ecole Polytechnique Fédérale de Lausanne (EPFL), Lausanne, Switzerland) for his help in building the ^{31}P coil.

References

[1] V. Mlynarik, I. Kohler, G. Gambarota, A. Vaslin, P.G. Clarke, R. Gruetter, Quantitative proton spectroscopic imaging of the neurochemical profile in rat brain with microliter resolution at ultra-short echo times, Magn. Reson Med. 59 (2008) 52–58.
[2] G. Oz, J.R. Alger, P.B. Barker, R. Bartha, A. Bizzi, C. Boesch, P.J. Bolan, K.M. Brindle, C. Cudalbu, A. Dincer, U. Dydak, U.E. Emir, J. Frahm, R.G. Gonzalez, S. Gruber, R. Gruetter, R.K. Gupta, A. Heerschap, A. Henning, H.P. Hetherington, F.A. Howe, P.S. Huppi, R.E. Hurd, K. Kantarci, D.W. Klomp, R. Kreis, M.J. Kruiskamp, M.O. Leach, A.P. Lin, P.R. Luijten, M. Marjanska, A.A. Maudsley, D.J. Meyerhoff, C.E. Mountford, S.J. Nelson, M.N. Pamir, J.W. Pan, A.C. Peet, H. Poptani, S. Posse, P.J. Pouwels, E.M. Ratai, B.D. Ross, T.W. Scheenen, C. Schuster, I.C. Smith, B.J. Soher, I. Tkac, D.B. Vigneron, R.A. Kauppinen, M.R.S.C. Group, Clinical proton MR spectroscopy in central nervous system disorders, Radiology 270 (2014) 658–679.
[3] O. Braissant, V.A. McLin, C. Cudalbu, Ammonia toxicity to the brain, J. Inherit. Metab. Dis. 36 (2013) 595–612.
[4] C. Bachmann, O. Braissant, A.M. Villard, O. Boulat, H. Henry, Ammonia toxicity to the brain and creatine, Mol Genet Metab 81 (Suppl 1) (2004) S52–S57.
[5] M.D. Norenberg, K.V. Rao, A.R. Jayakumar, Mechanisms of ammonia-induced astrocyte swelling, Metab. Brain Dis. 20 (2005) 303–318.
[6] M.D. Norenberg, K.V. Rama Rao, A.R. Jayakumar, Signaling factors in the mechanism of ammonia neurotoxicity, Metab. Brain Dis. 24 (2009) 103–117.
[7] D. Haussinger, G. Kircheis, R. Fischer, F. Schliess, S. Vom Dahl, Hepatic encephalopathy in chronic liver disease: a clinical manifestation of astrocyte swelling and low-grade cerebral edema? J. hepatology 32 (2000) 1035–1038.
[8] V. Felipo, R.F. Butterworth, Neurobiology of ammonia, Prog. Neurobiol. 67 (2002) 259–279.
[9] J. Cordoba, J. Gottstein, A.T. Blei, Glutamine, myo-inositol, and organic brain osmolytes after portocaval anastomosis in the rat: implications for ammonia-induced brain edema, Hepatology 24 (1996) 919–923.
[10] O. Braissant, L. Cagnon, F. Monnet-Tschudi, O. Speer, T. Wallimann, P. Honegger, H. Henry, Ammonium alters creatine transport and synthesis in a 3D culture of developing brain cells, resulting in secondary cerebral creatine deficiency, Eur. J. Neurosci. 27 (2008) 1673–1685.
[11] L. Cagnon, O. Braissant, Hyperammonemia-induced toxicity for the developing central nervous system, Brain Res. Rev. 56 (2007) 183–197.
[12] R.F. Butterworth, Hepatic encephalopathy, Alcohol Res. Health 27 (2003) 240–246.
[13] S.W. Brusilow, R. Traystman, Hepatic encephalopathy, N. Engl. J. Med. 314 (1986) 786–787.
[14] S.W. Brusilow, R.C. Koehler, R.J. Traystman, A.J.L. Cooper, Astrocyte glutamine synthetase: importance in hyperammonemic syndromes and potential target for therapy, Neurotherapeutics 7 (2010) 452–470.
[15] O. Braissant, Ammonia toxicity to the brain: effects on creatine metabolism and transport and protective roles of creatine, Mol. Genet. Metabolism 100 (Suppl 1) (2010) S53–S58.
[16] O. Braissant, Current concepts in the pathogenesis of urea cycle disorders, Mol. Genet. Metabolism 100 (Suppl 1) (2010) S3–S12.
[17] C. Bachmann, O. Braissant, A.M. Villard, O. Boulat, H. Henry, Ammonia toxicity to the brain and creatine, Mol Genet Metab 81 (Suppl 1) (2004) S52–S57.
[18] C. Bachmann, Mechanisms of hyperammonemia, Clin. Chem. Lab. Med. 40 (2002) 653–662.
[19] J. Albrecht, M.D. Norenberg, Glutamine: a Trojan horse in ammonia neurotoxicity, Hepatology 44 (2006) 788–794.
[20] A.J. Cooper, F. Plum, Biochemistry and physiology of brain ammonia, Physiol. Rev. 67 (1987) 440–519.
[21] M.D. Norenberg, Distribution of glutamine synthetase in the rat central nervous system, J. Histochem Cytochem 27 (1979) 756–762.
[22] R.F. Butterworth, Pathogenesis of hepatic encephalopathy: new insights from neuroimaging and molecular studies, J. hepatology 39 (2003) 278–285.
[23] M.D. Norenberg, K.V. Rama Rao, A.R. Jayakumar, Signaling factors in the mechanism of ammonia neurotoxicity, Metab. Brain Dis. 24 (2009) 103–117.
[24] R. Leke, L.K. Bak, M. Anker, T.M. Melo, M. Sorensen, S. Keiding, H. Vilstrup, P. Ott, L.V. Portela, U. Sonnewald, A. Schousboe, H.S. Waagepetersen, Detoxification of ammonia in mouse cortical GABAergic cell cultures increases neuronal oxidative metabolism and reveals an emerging role for release of glucose-derived alanine, Neurotox. Res. 19 (2011) 496–510.
[25] S.W. Brusilow, R. Traystman, Hepatic encephalopathy, N. Engl. J. Med. 314 (1986) 786–787 author reply 787.
[26] O. Cauli, P. Lopez-Larrubia, R. Rodrigo, A. Agusti, J. Boix, L. Nieto-Charques, S. Cerdan, V. Felipo, Brain region-selective mechanisms contribute to the progression of cerebral alterations in acute liver failure in rats, Gastroenterology 140 (2011) 638–645.
[27] O. Cauli, P. Lopez-Larrubia, T.B. Rodrigues, S. Cerdan, V. Felipo, Magnetic resonance analysis of the effects of acute ammonia intoxication on rat brain. Role of NMDA receptors, J. Neurochem. 103 (2007) 1334–1343.
[28] C. Cudalbu, V. Mlynárik, B. Lanz, H. Frenkel, N. Costers, R. Gruetter, Imaging glutamine synthesis rates in the hyperammonemic rat brain, Proc. Intl. Soc. Mag. Reson. Med. 18 (2010) 3324.
[29] S.M. Fitzpatrick, H.P. Hetherington, K.L. Behar, R.G. Shulman, Effects of acute hyperammonemia on cerebral amino acid metabolism and pHi in vivo, measured by 1H and 31P nuclear magnetic resonance, J. Neurochem. 52 (1989) 741–749.
[30] S.L. Nyberg, F.B. Cerra, R. Gruetter, Brain lactate by magnetic resonance spectroscopy during fulminant hepatic failure in the dog, Liver Transpl. Surg. 4 (1998) 158–165.
[31] J. Shen, N.R. Sibson, G. Cline, K.L. Behar, D.L. Rothman, R.G. Shulman, ^{15}N-NMR spectroscopy studies of ammonia transport and glutamine synthesis in the hyperammonemic rat brain, Dev. Neurosci. 20 (1998) 434–443.
[32] A. Rovira, J. Alonso, J. Cordoba, MR imaging findings in hepatic encephalopathy, AJNR Am. J. Neuroradiol. 29 (2008) 1612–1621.
[33] L. Spahr, P.R. Burkhard, H. Grotzsch, A. Hadengue, Clinical significance of basal ganglia alterations at brain MRI and 1H MRS in cirrhosis and role in the pathogenesis of hepatic encephalopathy, Metab. Brain Dis. 17 (2002) 399–413.
[34] S. Williams, Cerebral amino acids studied by nuclear magnetic resonance spectroscopy in vivo, Prog. Nucl. Magnetic Reson. Spectrosc. 34 (1999) 301–326.
[35] T.E. Bates, S.R. Williams, R.A. Kauppinen, D.G. Gadian, Observation of cerebral metabolites in an animal-model of acute liver-failure invivo - a H-1 and P-31 nuclear magnetic-resonance study, J. Neurochem. 53 (1989) 102–110.
[36] M.J. McPhail, S.D. Taylor-Robinson, The role of magnetic resonance imaging and spectroscopy in hepatic encephalopathy, Metab. Brain Dis. 25 (2010) 65–72.
[37] R. Kreis, N. Farrow, B.D. Ross, Localized 1H NMR spectroscopy in patients with chronic hepatic encephalopathy. Analysis of changes in cerebral glutamine, choline and inositols, NMR Biomed. 4 (1991) 109–116.
[38] R. Kreis, B.D. Ross, N.A. Farrow, Z. Ackerman, Metabolic disorders of the brain in chronic hepatic encephalopathy detected with H-1 MR spectroscopy, Radiology 182 (1992) 19–27.
[39] B.D. Ross, S. Jacobson, F. Villamil, J. Korula, R. Kreis, T. Ernst, T. Shonk, R.A. Moats, Subclinical hepatic encephalopathy: proton MR spectroscopic abnormalities, Radiology 193 (1994) 457–463.
[40] C. Cudalbu, V. Mlynarik, R. Gruetter, Handling macromolecule signals in the quantification of the neurochemical profile, J. Alzheimers Dis. 31 (Suppl 3) (2012) S101–S115.
[41] V. Govindaraju, K. Young, A.A. Maudsley, Proton NMR chemical shifts and coupling constants for brain metabolites, NMR Biomed. 13 (2000) 129–153.
[42] C.D. Rae, A guide to the metabolic pathways and function of metabolites observed in human brain H-1 magnetic resonance spectra, Neurochem. Res. 39 (2014) 1–36.
[43] R. Mekle, V. Mlynarik, G. Gambarota, M. Hergt, G. Krueger, R. Gruetter, MR spectroscopy of the human brain with enhanced signal intensity at ultrashort echo times on a clinical platform at 3T and 7T, Magn. Reson Med. 61 (2009) 1279–1285.
[44] V. Mlynarik, C. Cudalbu, L. Xin, R. Gruetter, 1H NMR spectroscopy of rat brain in vivo at 14.1Tesla: improvements in quantification of the neurochemical profile, J. Magn. Reson 194 (2008) 163–168.
[45] R. Bartha, D.J. Drost, R.S. Menon, P.C. Williamson, Comparison of the quantification precision of human short echo time (1)H spectroscopy at 1.5 and 4.0 Tesla, Magn. Reson Med. 44 (2000) 185–192.

[46] I. Tkac, G. Oz, G. Adriany, K. Ugurbil, R. Gruetter, In vivo 1H NMR spectroscopy of the human brain at high magnetic fields: metabolite quantification at 4T vs. 7T, Magn. Reson Med. 62 (2009) 868–879.
[47] G. Oz, I. Tkac, K. Ugurbil, Animal models and high field imaging and spectroscopy, Dialogues Clin. Neurosci. 15 (2013) 263–278.
[48] J. Pfeuffer, I. Tkac, S.W. Provencher, R. Gruetter, Toward an in vivo neurochemical profile: quantification of 18 metabolites in short-echo-time (1)H NMR spectra of the rat brain, J. magnetic Reson. 141 (1999) 104–120.
[49] I. Tkac, R. Gruetter, Methodology of H NMR spectroscopy of the human brain at very high magnetic fields, Appl. Magn. Reson 29 (2005) 139–157.
[50] I. Tkac, P. Andersen, G. Adriany, H. Merkle, K. Ugurbil, R. Gruetter, In vivo 1H NMR spectroscopy of the human brain at 7 T, Magn. Reson Med. 46 (2001) 451–456.
[51] I. Tkac, P.G. Henry, P. Andersen, C.D. Keene, W.C. Low, R. Gruetter, Highly resolved in vivo 1H NMR spectroscopy of the mouse brain at 9.4 T, Magn. Reson Med. 52 (2004) 478–484.
[52] D.K. Deelchand, I. Iltis, P.G. Henry, Improved quantification precision of human brain short echo-time (1) H magnetic resonance spectroscopy at high magnetic field: a simulation study, Magn. Reson Med. 72 (2014) 20–25.
[53] J. Frahm, H. Bruhn, M.L. Gyngell, K.D. Merboldt, W. Hanicke, R. Sauter, Localized proton NMR spectroscopy in different regions of the human brain in vivo. Relaxation times and concentrations of cerebral metabolites, Magn. Reson Med. 11 (1989) 47–63.
[54] V. Mlynarik, S. Gruber, E. Moser, Proton T (1) and T (2) relaxation times of human brain metabolites at 3 Tesla, NMR Biomed. 14 (2001) 325–331.
[55] L. Hofmann, J. Slotboom, B. Jung, P. Maloca, C. Boesch, R. Kreis, Quantitative 1H-magnetic resonance spectroscopy of human brain: influence of composition and parameterization of the basis set in linear combination model-fitting, Magn. Reson Med. 48 (2002) 440–453.
[56] R. Kreis, Issues of spectral quality in clinical 1H-magnetic resonance spectroscopy and a gallery of artifacts, NMR Biomed. 17 (2004) 361–381.
[57] R. Gruetter, I. Tkac, Field mapping without reference scan using asymmetric echo-planar techniques, Magn. Reson Med. 43 (2000) 319–323.
[58] R. Gruetter, Automatic, localized invivo adjustment of all 1st-order and 2nd-order shim coils, Magn. Reson Med. 29 (1993) 804–811.
[59] C. Juchem, P.B. Brown, T.W. Nixon, S. McIntyre, D.L. Rothman, R.A. de Graaf, Multicoil shimming of the mouse brain, Magn. Reson Med. 66 (2011) 893–900.
[60] C. Juchem, P. Herman, B.G. Sanganahalli, P.B. Brown, S. McIntyre, T.W. Nixon, D. Green, F. Hyder, R.A. de Graaf, DYNAmic Multi-coil TEchnique (DYNAMITE) shimming of the rat brain at 11.7 T, NMR Biomed. 27 (2014) 897–906.
[61] O. Reynaud, D. Gallichan, B. Schaller, R. Gruetter, Fast low-specific absorption rate B0 -mapping along projections at high field using two-dimensional radiofrequency pulses, Magn. Reson Med. 73 (2015) 901–908.
[62] I. Tkac, Z. Starcuk, I.Y. Choi, R. Gruetter, In vivo 1H NMR spectroscopy of rat brain at 1 ms echo time, Magn. Reson Med. 41 (1999) 649–656.
[63] H. Lei, L. Xin, R. Gruetter, M. Mlynarik, Localized single voxel magnetic resonance spectroscopy, water suppression, and novel approaches for ultrashort echo-time measurements, in: D. Rothman, C. Stagg (Eds.), Magnetic Resonance Spectroscopy, Elsevier, Oxford:Academic Press, 2013, pp. 15–30.
[64] M. Gottschalk, L. Lamalle, C. Segebarth, Short-TE localised 1H MRS of the human brain at 3 T: quantification of the metabolite signals using two approaches to account for macromolecular signal contributions, NMR Biomed. 21 (2008) 507–517.
[65] C. Cudalbu, V. Mlynarik, L. Xin, R. Gruetter, Comparison of two approaches to model the macromolecule spectrum for the quantification of short TE H-1 MRS spectra, I W Imag. Syst. Tech. (2008) 309–312.
[66] C. Cudalbu, V. Mlynarik, L. Xin, R. Gruetter, Quantification of in vivo short echo-time proton magnetic resonance spectra at 14.1 T using two different approaches of modelling the macromolecule spectrum, Meas. Sci. Technol. 20 (2009) 104034.
[67] C. Cudalbu, A. Bucur, D. Graveron-Demilly, O. Beuf, S. Cavassila, Comparison of two strategies of background-accommodation: influence on the metabolite concentration estimation from in vivo Magnetic Resonance Spectroscopy data, Conf. Proc. IEEE Eng. Med. Biol. Soc. 2007 (2007) 2077–2080.
[68] C. Cudalbu, S. Cavassila, H. Rabeson, D. van Ormondt, D. Graveron-Demilly, Influence of measured and simulated basis sets on metabolite concentration estimates, NMR Biomed. 21 (2008) 627–636.
[69] D. van Ormondt, D. Graveron-Demilly, D.M. Sima, S. Van Huffel, S.R. Williams, Time-Domain Methods Quantifying MR Spectra eMagRes 4 (2015) 651–662.
[70] A. Henning, Advanced spectral quantification: parameter handling, nonparametric pattern modeling, and multidimensional fitting, eMagRes 5 (2016) 981–994.
[71] S. Cavassila, S. Deval, C. Huegen, D. van Ormondt, D. Graveron-Demilly, Cramer-Rao bounds: an evaluation tool for quantitation, NMR Biomed. 14 (2001) 278–283.
[72] S. Cavassila, S. Deval, C. Huegen, D. van Ormondt, D. Graveron-Demilly, Cramer-Rao bound expressions for parametric estimation of overlapping peaks: influence of prior knowledge, J. magnetic Reson. 143 (2000) 311–320.
[73] R. Kreis, The trouble with quality filtering based on relative Cramer-Rao lower bounds, Magn. Reson Med. 75 (2016) 15–18.
[74] C. Cudalbu, S. Cavassila, H. Rabeson, D. van Ormonde, D. Graveron-Demilly, Influence of measured and simulated basis sets on metabolite concentration estimates, NMR Biomed 21 (2008) 627–636.
[75] G. Helms, The principles of quantification applied to in vivo proton MR spectroscopy, Eur. J. Radiol. 67 (2008) 218–229.
[76] P.K. Mandal, In vivo proton magnetic resonance spectroscopic signal processing for the absolute quantitation of brain metabolites, Eur. J. Radiol. 81 (4) (2012) e653–e664.
[77] J.B. Poullet, D.M. Sima, A.W. Simonetti, B. De Neuter, L. Vanhamme, P. Lemmerling, S. Van Huffel, An automated quantitation of short echo time MRS spectra in an open source software environment: AQSES, NMR Biomed. 20 (2007) 493–504.
[78] J.B. Poullet, D.M. Sima, S. Van Huffel, Frequency-selective quantification of short-echo time magnetic resonance spectra, Conf. Proc. IEEE Eng. Med. Biol. Soc. 1 (2006) 6351–6355.
[79] J.B. Poullet, D.M. Sima, S. Van Huffel, MRS signal quantitation: a review of time- and frequency-domain methods, J. magnetic Reson. 195 (2008) 134–144.
[80] H. Ratiney, M. Sdika, Y. Coenradie, S. Cavassila, D. van Ormondt, D. Graveron-Demilly, Time-domain semi-parametric estimation based on a metabolite basis set, NMR Biomed. 18 (2005) 1–13.
[81] J. Slotboom, C. Boesch, R. Kreis, Versatile frequency domain fitting using time domain models and prior knowledge, Magn. Reson Med. 39 (1998) 899–911.
[82] T. Ernst, R. Kreis, B.D. Ross, Absolute quantitation of water and metabolites in the human brain. I. Compartments and water, J. Magnetic Reson. Ser. B 102 (1993) 1–8.
[83] T. Ernst, R. Kreis, B.D. Ross, Absolute quantitation of water and metabolites in the human brain. II. Metabolite concentrations, J. Magnetic Reson. Ser. B 102 (1993) 9–19.
[84] C. Cudalbu, B. Lanz, J.M. Duarte, F.D. Morgenthaler, Y. Pilloud, V. Mlynarik, R. Gruetter, Cerebral glutamine metabolism under hyperammonemia determined in vivo by localized (1)H and (15)N NMR spectroscopy, J. Cereb. Blood Flow. Metab. 32 (2012) 696–708.
[85] R. Gruetter, G. Adriany, I.Y. Choi, P.G. Henry, H. Lei, G. Oz, Localized in vivo 13C NMR spectroscopy of the brain, NMR Biomed. 16 (2003) 313–338.
[86] R.A. De Graaf, In Vivo NMR Spectroscopy – 2nd Edition: Principles and Techniques, John Wiley & Sons Ltd, 2007.
[87] R.A. de Graaf, P.B. Brown, S. McIntyre, T.W. Nixon, K.L. Behar, D.L. Rothman, High magnetic field water and metabolite proton T1 and T2 relaxation in rat brain in vivo, Magn. Reson Med. 56 (2006) 386–394.
[88] C. Cudalbu, V. Mlynarik, L. Xin, R. Gruetter, Comparison of T1 relaxation times of the neurochemical profile in rat brain at 9.4 tesla and 14.1 tesla, Magn. Reson Med. 62 (2009) 862–867.
[89] L. Chavarria, M. Oria, J. Romero-Gimenez, J. Alonso, S. Lope-Piedrafita, J. Cordoba, Diffusion tensor imaging supports the cytotoxic origin of brain edema in a rat model of acute liver failure, Gastroenterology 138 (2010) 1566–1573.
[90] D.K. Bosman, N.E. Deutz, A.A. De Graaf, R.W. vd Hulst, H.M. Van Eijk, W.M. Bovee, M.A. Maas, G.G. Jorning, R.A. Chamuleau, Changes in brain metabolism during hyperammonemia and acute liver failure: results of a comparative 1H-NMR spectroscopy and biochemical investigation, Hepatology 12 (1990) 281–290.
[91] N. Chatauret, C. Zwingmann, C. Rose, D. Leibfritz, R.F. Butterworth, Effects of hypothermia on brain glucose metabolism in acute liver failure: a H/C-nuclear magnetic resonance study, Gastroenterology 125 (2003) 815–824.
[92] B. Hindfelt, F. Plum, T.E. Duffy, Effect of acute ammonia intoxication on cerebral metabolism in rats with portacaval shunts, J. Clin. Invest. 59 (1977) 386–396.
[93] R.F. Butterworth, M.D. Norenberg, V. Felipo, P. Ferenci, J. Albrecht, A.T. Blei, I.C.o.E.M.o.H.E. Members of the, Experimental models of hepatic encephalopathy: ISHEN guidelines, Liver Int. official J. Int. Assoc. Study Liver 29 (2009) 783–788.
[94] C. Cudalbu, In vivo studies of brain metabolism in animal models of Hepatic Encephalopathy using (1)H Magnetic Resonance Spectroscopy, Metab. Brain Dis. 28 (2013) 167–174.
[95] V. Rackayova, O. Braissant, V.A. McLin, C. Berset, B. Lanz, C. Cudalbu, 1H and 31P magnetic resonance spectroscopy in a rat model of chronic hepatic encephalopathy: in vivo longitudinal measurements of brain energy metabolism, Metab. Brain Dis. 31 (6) (2016) 1303–1314.
[96] L. Chavarria, J. Cordoba, Magnetic resonance of the brain in chronic and acute liver failure, Metab. Brain Dis. 29 (2014) 937–944.
[97] L. Chavarria, M. Oria, J. Romero-Gimenez, J. Alonso, S. Lope-Piedrafita, J. Cordoba, Brain magnetic resonance in experimental acute-on-chronic liver failure, Liver Int. official J. Int. Assoc. Study Liver 33 (2013) 294–300.
[98] J. Cordoba, J. Gottstein, A.T. Blei, Chronic hyponatremia exacerbates ammonia-induced brain edema in rats after portacaval anastomosis, J. hepatology 29 (1998) 589–594.
[99] J. Cordoba, Glutamine, myo-inositol, and brain edema in acute liver failure, Hepatology 23 (1996) 1291–1292.
[100] C. Cudalbu, O. Braissant, M. Lepore, R. Gruetter, V.A. McLin, in: Brain osmolytes and brain edema in a rat model of chronic liver failure: in vivo longitudinal 1H spectroscopic imaging and diffusion tensor imaging studies at 9.4T, 15th ISHEN Symposium, O7, 2012.
[101] S. Berl, G. Takagaki, D.D. Clarke, H. Waelsch, Metabolic compartments in vivo. Ammonia and glutamic acid metabolism in brain and liver, J. Biol. Chem. 237 (1962) 2562–2569.
[102] C. Zwingmann, The anaplerotic flux and ammonia detoxification in hepatic encephalopathy, Metab. Brain Dis. 22 (2007) 235–249.
[103] K. Kanamori, F. Parivar, B.D. Ross, A 15N NMR study of in vivo cerebral

glutamine synthesis in hyperammonemic rats, NMR Biomed. 6 (1993) 21–26.
[104] K. Kanamori, B.D. Ross, 15N n.m.r. measurement of the in vivo rate of glutamine synthesis and utilization at steady state in the brain of the hyperammonaemic rat, Biochem. J. 293 (Pt 2) (1993) 461–468.
[105] K. Kanamori, B.D. Ross, J.C. Chung, E.L. Kuo, Severity of hyperammonemic encephalopathy correlates with brain ammonia level and saturation of glutamine synthetase in vivo, J. Neurochem. 67 (1996) 1584–1594.
[106] O. Braissant, Ammonia toxicity to the brain: effects on creatine metabolism and transport and protective roles of creatine, Mol Genet Metab 100 (Suppl 1) (2010) S53–S58.
[107] B. Lanz, R. Gruetter, J.M. Duarte, Metabolic Flux, Compartmentation, Analysis in the brain, Front. Endocrinol. 4 (2013) 156.
[108] G. Siegel, S. Brady, R.W. Albers, D. Price, Basic neurochemistry: principles of molecular, cellular, and medical neurobiology, Elsevier Science, 2011.
[109] B. Thorens, M. Mueckler, Glucose transporters in the 21st century, Am. J. physiology 298 (2010) E141–E145.
[110] A.P. Halestrap, N.T. Price, The proton-linked monocarboxylate transporter (MCT) family: structure, function and regulation, Biochem. J. 343 Pt (2) (1999) 281–299.
[111] A. Nehlig, E. Wittendorp-Rechenmann, C.D. Lam, Selective uptake of [14C]2-deoxyglucose by neurons and astrocytes: high-resolution microautoradiographic imaging by cellular 14C-trajectography combined with immunohistochemistry, J. Cereb. Blood Flow. Metab. 24 (2004) 1004–1014.
[112] P.J. Magistretti, L. Pellerin, D.L. Rothman, R.G. Shulman, Energy on demand, Science 283 (1999) 496–497.
[113] R. Gruetter, Glycogen: the forgotten cerebral energy store, J. Neurosci. Res. 74 (2003) 179–183.
[114] R.A. Waniewski, D.L. Martin, Preferential utilization of acetate by astrocytes is attributable to transport, J. Neurosci. 18 (1998) 5225–5233.
[115] R. Gruetter, E.R. Seaquist, K. Ugurbil, A mathematical model of compartmentalized neurotransmitter metabolism in the human brain, Am. J. physiology 281 (2001) E100–E112.
[116] R.A. De Graaf, In Vivo NMR Spectroscopy: Principles and Techniques, John Wiley & Sons, 2008.
[117] S. Berl, G. Takagaki, D.D. Clarke, H. Waelsch, Carbon dioxide fixation in the brain, J. Biol. Chem. 237 (1962) 2570–2573.
[118] R.S. Badar-Goffer, H.S. Bachelard, P.G. Morris, Cerebral metabolism of acetate and glucose studied by 13C-n.m.r. spectroscopy. A technique for investigating metabolic compartmentation in the brain, Biochem. J. 266 (1990) 133–139.
[119] D. Ebert, R.G. Haller, M.E. Walton, Energy contribution of octanoate to intact rat brain metabolism measured by 13C nuclear magnetic resonance spectroscopy, J. Neurosci. 23 (2003) 5928–5935.
[120] L. Hertz, Functional interactions between neurons and astrocytes I. Turnover and metabolism of putative amino acid transmitters, Prog. Neurobiol. 13 (1979) 277–323.
[121] A. Martinez-Hernandez, K.P. Bell, M.D. Norenberg, Glutamine synthetase: glial localization in brain, Science 195 (1977) 1356–1358.
[122] A.J. Patel, A. Hunt, R.D. Gordon, R. Balazs, The activities in different neural cell types of certain enzymes associated with the metabolic compartmentation glutamate, Brain Res. 256 (1982) 3–11.
[123] O.P. Ottersen, N. Zhang, F. Walberg, Metabolic compartmentation of glutamate and glutamine: morphological evidence obtained by quantitative immunocytochemistry in rat cerebellum, Neuroscience 46 (1992) 519–534.
[124] A.J. Cooper, J.M. McDonald, A.S. Gelbard, R.F. Gledhill, T.E. Duffy, The metabolic fate of 13N-labeled ammonia in rat brain, J. Biol. Chem. 254 (1979) 4982–4992.
[125] I. Zaganas, H.S. Waagepetersen, P. Georgopoulos, U. Sonnewald, A. Plaitakis, A. Schousboe, Differential expression of glutamate dehydrogenase in cultured neurons and astrocytes from mouse cerebellum and cerebral cortex, J. Neurosci. Res. 66 (2001) 909–913.
[126] S.P. Bessman, A.N. Bessman, The cerebral and peripheral uptake of ammonia in liver disease with an hypothesis for the mechanism of hepatic coma, J. Clin. Invest. 34 (1955) 622–628.
[127] A.J. Cooper, T.M. Jeitner, Central role of glutamate metabolism in the maintenance of nitrogen homeostasis in normal and hyperammonemic brain, Biomolecules 6 (2016).
[128] N.R. Sibson, A. Dhankhar, G.F. Mason, K.L. Behar, D.L. Rothman, R.G. Shulman, In vivo ^{13}C NMR measurements of cerebral glutamine synthesis as evidence for glutamate-glutamine cycling, Proceedings National Academy Sciences United States of America 94 (1997) 2699–2704.
[129] C. Zwingmann, N. Chatauret, D. Leibfritz, R.F. Butterworth, Selective increase of brain lactate synthesis in experimental acute liver failure: results of a [H-C] nuclear magnetic resonance study, Hepatology 37 (2003) 420–428.
[130] R. Badar-Goffer, H. Bachelard, Metabolic studies using 13C nuclear magnetic resonance spectroscopy, Essays Biochem. 26 (1991) 105–119.
[131] C.R. Bosoi, C. Zwingmann, H. Marin, C. Parent-Robitaille, J. Huynh, M. Tremblay, C.F. Rose, Increased brain lactate is central to the development of brain edema in rats with chronic liver disease, J. hepatology 60 (2014) 554–560.
[132] C. Zwingmann, D. Leibfritz, Ammonia toxicity under hyponatremic conditions in astrocytes: de novo synthesis of amino acids for the osmoregulatory response, Neurochem. Int. 47 (2005) 39–50.
[133] R.F. Butterworth, Pathophysiology of brain dysfunction in hyperammonemic syndromes: the many faces of glutamine, Mol. Genet. metabolism 113 (2014) 113–117.
[134] J.M.N. Duarte, B. Lanz, R. Gruetter, Compartmentalized cerebral metabolism of [1,6–13C]glucose determined by in vivo 13C NMR spectroscopy at 14.1 T, Front. neuroenergetics 3 (2011).
[135] B. Lanz, L. Xin, P. Millet, R. Gruetter, In vivo quantification of neuro-glial metabolism and glial glutamate concentration using 1H-[13C] MRS at 14.1T, J. Neurochem. 128 (1) (2014) 125–139.
[136] R. Gruetter, In vivo 13C NMR studies of compartmentalized cerebral carbohydrate metabolism, Neurochem. Int. 41 (2002) 143–154.
[137] D.L. Rothman, H.M. De Feyter, R.A. de Graaf, G.F. Mason, K.L. Behar, 13C MRS studies of neuroenergetics and neurotransmitter cycling in humans, NMR Biomed. 24 (2011) 943–957.
[138] P.G. Henry, G. Adriany, D. Deelchand, R. Gruetter, M. Marjanska, G. Oz, E.R. Seaquist, A. Shestov, K. Ugurbil, In vivo 13C NMR spectroscopy and metabolic modeling in the brain: a practical perspective, Magn. Reson. imaging 24 (2006) 527–539.
[139] B. Lanz, J.M. Duarte, N. Kunz, V. Mlynarik, R. Gruetter, C. Cudalbu, Which prior knowledge? Quantification of in vivo brain 13C MR spectra following 13C glucose infusion using AMARES, Magn. Reson Med. 69 (2013) 1512–1522.
[140] R. Gruetter, E.J. Novotny, S.D. Boulware, G.F. Mason, D.L. Rothman, G.I. Shulman, J.W. Prichard, R.G. Shulman, Localized 13C NMR spectroscopy in the human brain of amino acid labeling from D-[1-13C]glucose, J. Neurochem. 63 (1994) 1377–1385.
[141] G.F. Mason, R. Gruetter, D.L. Rothman, K.L. Behar, R.G. Shulman, E.J. Novotny, Simultaneous determination of the rates of the TCA cycle, glucose utilization, alpha-ketoglutarate/glutamate exchange, and glutamine synthesis in human brain by NMR, J. Cereb. Blood Flow. Metab. 15 (1995) 12–25.
[142] G.F. Mason, D.L. Rothman, K.L. Behar, R.G. Shulman, NMR determination of the TCA cycle rate and alpha-ketoglutarate/glutamate exchange rate in rat brain, J. Cereb. Blood Flow. Metab. 12 (1992) 434–447.
[143] D.L. Rothman, E.J. Novotny, G.I. Shulman, A.M. Howseman, O.A. Petroff, G. Mason, T. Nixon, C.C. Hanstock, J.W. Prichard, R.G. Shulman, 1H-[13C] NMR measurements of [4-13C]glutamate turnover in human brain, Proceedings National Academy Sciences United States of America 89 (1992) 9603–9606.
[144] N.R. Sibson, G.F. Mason, J. Shen, G.W. Cline, A.Z. Herskovits, J.E. Wall, K.L. Behar, D.L. Rothman, R.G. Shulman, In vivo ^{13}C NMR measurement of neurotransmitter glutamate cycling, anaplerosis and TCA cycle flux in rat brain during [2-13C]glucose infusion, J. Neurochem. 76 (2001) 975–989.
[145] J.L. Arriza, W.A. Fairman, J.I. Wadiche, G.H. Murdoch, M.P. Kavanaugh, S.G. Amara, Functional comparisons of three glutamate transporter subtypes cloned from human motor cortex, J. Neurosci. 14 (1994) 5559–5569.
[146] M. De Pitta, V. Volman, H. Berry, E. Ben-Jacob, A tale of two stories: astrocyte regulation of synaptic depression and facilitation, PLoS Comput. Biol. 7 (2011) e1002293.
[147] L. Xin, V. Mlynarik, B. Lanz, H. Frenkel, R. Gruetter, 1H-[13C] NMR spectroscopy of the rat brain during infusion of [2-13C] acetate at 14.1 T, Magn. Reson Med. 64 (2010) 334–340.
[148] L. Vanhamme, A. van den Boogaart, S. Van Huffel, Improved method for accurate and efficient quantification of MRS data with use of prior knowledge, J. Magn. Reson 129 (1997) 35–43.
[149] K. Kanamori, B.D. Ross, Steady-state in vivo glutamate dehydrogenase activity in rat brain measured by 15N NMR, J. Biol. Chem. 270 (1995) 24805–24809.
[150] C.R. Bosoi, C.F. Rose, Identifying the direct effects of ammonia on the brain, Metab. Brain Dis. 24 (2009) 95–102.
[151] I.Y. Choi, I. Tkac, R. Gruetter, Single-shot, three-dimensional “non-echo” localization method for in vivo NMR spectroscopy, Magn. Reson Med. 44 (2000) 387–394.
[152] K. Uffmann, R. Gruetter, Mathematical modeling of (13)C label incorporation of the TCA cycle: the concept of composite precursor function, J. Neurosci. Res. 85 (2007) 3304–3317.
[153] J.M.N. Duarte, B.,G.R. Lanz, Compartmentalised cerebral metabolism of [1,6-13C]glucose determined by in vivo 13C NMR spectroscopy at 14.1 T, Front. neuroenergetics 3 (2011) 3.
[154] I. Tkac, P.G. Henry, L. Zacharoff, M. Wedel, W. Gong, D.K. Deelchand, T. Li, J.M. Dubinsky, Homeostatic adaptations in brain energy metabolism in mouse models of Huntington disease, J. Cereb. Blood Flow. Metab. 32 (2012) 1977–1988.
[155] S. Nioka, B. Chance, M. Hilberman, H.V. Subramanian, J.S. Leigh Jr., R.L. Veech, R.E. Forster, Relationship between intracellular pH and energy metabolism in dog brain as measured by 31P-NMR, J. Appl. physiology 62 (1987) 2094–2102.
[156] R.L. Veech, J.W. Lawson, N.W. Cornell, H.A. Krebs, Cytosolic phosphorylation potential, J. Biol. Chem. 254 (1979) 6538–6547.
[157] D.K. Deelchand, T.M. Nguyen, X.H. Zhu, F. Mochel, P.G. Henry, Quantification of in vivo (3)(1)P NMR brain spectra using LCModel, NMR Biomed. 28 (2015) 633–641.
[158] K.V. Rama Rao, M.D. Norenberg, Brain energy metabolism and mitochondrial dysfunction in acute and chronic hepatic encephalopathy, Neurochem. Int. 60 (2012) 697–706.
[159] S. Bluml, E. Zuckerman, J. Tan, B.D. Ross, Proton-decoupled 31P magnetic resonance spectroscopy reveals osmotic and metabolic disturbances in

human hepatic encephalopathy, J. Neurochem. 71 (1998) 1564–1576.
[160] S.D. Taylor-Robinson, J. Sargentoni, A. Oatridge, D.J. Bryant, J.V. Hajnal, C.D. Marcus, J.P. Seery, H.J. Hodgson, N.M. deSouza, MR imaging and spectroscopy of the basal ganglia in chronic liver disease: correlation of T1-weighted contrast measurements with abnormalities in proton and phosphorus-31 MR spectra, Metab. Brain Dis. 11 (1996) 249–268.
[161] S.D. Taylor-Robinson, C. Buckley, K.K. Changani, H.J. Hodgson, J.D. Bell, Cerebral proton and phosphorus-31 magnetic resonance spectroscopy in patients with subclinical hepatic encephalopathy, Liver 19 (1999) 389–398.
[162] B. Barbiroli, S. Gaiani, R. Lodi, S. Iotti, C. Tonon, V. Clementi, G. Donati, L. Bolondi, Abnormal brain energy metabolism shown by in vivo phosphorus magnetic resonance spectroscopy in patients with chronic liver disease, Brain Res. Bull. 59 (2002) 75–82.
[163] O.A. Petroff, J.W. Prichard, K.L. Behar, J.R. Alger, J.A. den Hollander, R.G. Shulman, Cerebral intracellular pH by 31P nuclear magnetic resonance spectroscopy, Neurology 35 (1985) 781–788.
[164] S. Iotti, C. Frassineti, L. Alderighi, A. Sabatini, A. Vacca, B. Barbiroli, In vivo assessment of free magnesium concentration in human brain by 31P MRS. A new calibration curve based on a mathematical algorithm, NMR Biomed. 9 (1996) 24–32.
[165] E.M. Golding, W.E. Teague Jr., G.P. Dobson, Adjustment of K' to varying pH and pMg for the creatine kinase, adenylate kinase and ATP hydrolysis equilibria permitting quantitative bioenergetic assessment, J. Exp. Biol. 198 (1995) 1775–1782.
[166] S. Nioka, B. Chance, M. Hilberman, H.V. Subramanian, J.S. Leigh, R.L. Veech, R.E. Forster, Relationship between intracellular pH and energy metabolism in dog brain as measured by 31P-NMR, J. Appl. physiology 62 (1987) 2094–2102.
[167] S.A. Kuby, L. Noda, H.A. Lardy, Adenosinetriphosphate-creatine transphosphorylase. III. Kinetic studies, J. Biol. Chem. 210 (1954) 65–82.